

Supporting Information

Reconstructions of electron density by the Maximum Entropy Method from X-ray powder diffraction data based on incomplete and complete crystal structure models: a case study of apatites with different intercalated metal atoms.

Oxana V. Magdysyuk¹, Robert E. Dinnebier^{*1}, Sander van Smaalen², Mikhail A. Zykin³, Pavel E. Kazin⁴, Martin Jansen¹.

- [1] Max Planck Institute for Solid State Research,
70569 Stuttgart, Germany
- [2] Laboratory of Crystallography, University of Bayreuth,
95440 Bayreuth, Germany
- [3] Department of Materials Science, Moscow State University
119991 Moscow, Russia
- [4] Department of Chemistry, Moscow State University
119991 Moscow, Russia

* Correspondence author (e-mail: R.Dinnebier@fkf.mpg.de)

Table of contents

Section S1. Experimental and calculation procedures

Section S2. Examples of Rietveld refinement and Le Bail fit

Section S3. Localization of missing intercalated metal atoms from laboratory X-ray powder diffraction data

Section S4. Localization of missing intercalated metal atoms from synchrotron X-ray powder diffraction data

Section S5. Determination of the electron density distribution from synchrotron X-ray powder diffraction data

Section S6. Crystallographic and refinement data (Rietveld refinement and Le Bail fit of incomplete crystal structures without intercalated metal atoms) for hydroxyapatites with different intercalated metal atoms from laboratory and synchrotron X-ray powder diffraction data

Section S7. Crystallographic and refinement data (Rietveld refinement of complete crystal structures) for hydroxyapatites with different intercalated metal atoms from laboratory and synchrotron X-ray powder diffraction data

Section S8. Details about maximum-entropy calculations (based on $F_{\text{obs}}+G$) for incomplete crystal structures (without intercalated metal atoms) of investigated apatites from laboratory and synchrotron X-ray powder diffraction data.

Section S9. Details about maximum-entropy calculations (based on $F_{\text{obs}}+G$) for complete crystal structures of investigated apatites from laboratory and synchrotron X-ray powder diffraction data.

Section S10. References

Section S1. Experimental and calculation procedures.

X-ray powder diffraction data of 17 hydroxyapatite compounds with intercalated copper atoms were collected at room temperature on a laboratory powder diffractometer D8–Advance (Cu–K α_1 radiation from a primary Ge(111) monochromator; Linx-Eye position-sensitive detector with 3.5° 2 θ opening) in Bragg-Brentano geometry. The samples were rotated during the measurement for better particle statistics. For the present study, five series of apatites were selected:

a) Sr–hydroxyapatites (SrA) without fluorine atoms with different content of intercalated copper atoms: Sr₅(PO₄)₃Cu_{0.3}OH_{0.7- δ} (sample SrA(0.3Cu-2), δ = 0.104), Sr₅(PO₄)₃Cu_{0.25}OH_{0.75- δ} (sample SrA(0.25Cu)), Sr₅(PO₄)₃Cu_{0.125}OH_{0.875- δ} (sample SrA(0.125Cu)), Sr₅(PO₄)₃Cu_{0.1}OH_{0.9- δ} (sample SrA(0.1Cu-2), δ = 0.10), Sr₅(PO₄)₃Cu_{0.05}OH_{0.95- δ} (sample SrA(0.05Cu)).

b) Ca–hydroxyapatites (CaA) without fluorine atoms with different content of intercalated copper atoms: Ca₅(PO₄)₃Cu_{0.3}OH_{0.7- δ} (sample CaA(0.3Cu)), Ca₅(PO₄)₃Cu_{0.1}OH_{0.9- δ} (sample CaA(0.1Cu)).

c) Ca– and Sr–hydroxyapatites (CaA and SrA) with in-channel fluorine atoms and with different content of intercalated copper atoms: Ca₅(PO₄)₃Cu_{0.1}O_{0.5}H_{0.4- δ} F_{0.5} (sample CaA(0.1Cu_0.5F)), Ca₅(PO₄)₃Cu_{0.05}O_{0.5}H_{0.45- δ} F_{0.5} (sample CaA(0.05Cu_0.5F)), Ca₅(PO₄)₃Cu_{0.02}O_{0.5}H_{0.48- δ} F_{0.5} (sample CaA(0.02Cu_0.5F)), Ca₅(PO₄)₃Cu_{0.01}O_{0.5}H_{0.49- δ} F_{0.5} (sample CaA(0.01Cu_0.5F)), Sr₅(PO₄)₃Cu_{0.05}O_{0.5}H_{0.45- δ} F_{0.5} (sample SrA(0.05Cu_0.5F)).

d) Sr–hydroxyapatites (SrA) with intercalated copper atoms of occupancy 0.1 and different content (δ) of peroxide and/or copper ions in higher oxidation state:

Sr₅(PO₄)₃Cu_{0.1}OH_{0.9- δ} (sample SrA(0.1Cu-1), δ = 0.038), Sr₅(PO₄)₃Cu_{0.1}OH_{0.9- δ} (sample SrA(0.1Cu-2), δ = 0.10), Sr₅(PO₄)₃Cu_{0.1}OH_{0.9- δ} (sample SrA(0.1Cu-3), δ = 0.26), Sr₅(PO₄)₃Cu_{0.1}OH_{0.9- δ} (sample SrA(0.1Cu-4), δ > 0.26).

e) Sr–hydroxyapatites (SrA) with intercalated copper atoms of occupancy 0.3 and different content (δ) of peroxide and copper ions in higher oxidation state:

Sr₅(PO₄)₃Cu_{0.3}OH_{0.7- δ} (sample SrA(0.3Cu-1), δ = 0.022), Sr₅(PO₄)₃Cu_{0.3}OH_{0.7- δ} (sample SrA(0.3Cu-2), δ = 0.104), Sr₅(PO₄)₃Cu_{0.3}OH_{0.7- δ} (sample SrA(0.3Cu-3), δ = 0.29).

Parameter δ corresponds to the presence of peroxide ions O_2^{2-} (equivalent to $\frac{1}{2} \delta$) and/or copper in the oxidation state above +1 (equivalent to $\frac{\delta}{n-1}$, n – the copper oxidation state).

X-ray powder diffraction data of one series (d) of Sr-apatites were also measured at room temperature at the high-resolution powder diffractometer on I11 at Diamond (Parker et al., 2011; Thompson et al., 2011; Thompson et al., 2009). The wavelength was determined to be 0.8264(3) Å from a silicon standard. The samples were contained in sealed 0.5-mm lithium borate glass capillaries and were rotated around θ in order to improve randomization of the crystallites. The diffracted beam was detected with 45 MAC detectors. The sample SrA(0.1Cu-1) changed color from almost white to light blue-violet during the measurement which can be attributed to oxidation of intercalated copper atoms. All other samples did not show any visible color change.

Preparation and properties of samples of series a), b) and c) were published in Karpov et al. (2003), Kazin et al. (2003), Kazin et al. (2008), of series d) and e) will be published elsewhere (Kazin et al.)

X-ray powder diffraction data of two hydroxyapatites with intercalated nickel and zinc atoms were collected at room temperature on a laboratory powder diffractometer STOE (Cu-K α_1 radiation from a primary Ge(111) monochromator; Mythen-Dectris) in Debye-Scherrer geometry. The samples were rotated during the measurement for better particle statistics. For the present study, two apatites were used: $Sr_5(PO_4)_3Ni_{0.2}OH_{0.8-\delta}$ (sample SrA(0.2Ni)) and $Sr_5(PO_4)_3Zn_{0.15}OH_{0.85-\delta}$ (sample SrA(0.15Zn)). Preparation and properties of Sr-hydroxyapatites with the intercalated nickel and zinc atoms were published in Kazin et al. (2007).

The program Topas 4.1 (TOPAS version 4.1, 2007) was used for extraction of intensities after whole powder pattern fitting (WPPF) according to the Rietveld or Le Bail method. The fundamental-parameter approach to line profile analysis (Cheary et al., 1992), implemented in Topas 4.1, allows to describe accurately line profile shapes across a large 2θ range, and all refined parameter values have physical meaning. In the conventional mathematical approach to fitting, the refined numerical parameters have limited physical meaning, which can be responsible for an erroneous assigning of

intensities in groups of overlapping reflections in the latter approach. Crystallographic and refinement data for all samples at ambient conditions are given in Tables S6.1-S6.2 and S7.1-S7.2. Experimental and calculated profiles for typical Rietveld refinements and Le Bail fits are given in figs. S2.1 and S2.2.

All MEM calculations were performed with the computer program BayMEM (van Smaalen et al., 2003), employing the Sakata–Sato algorithm (Sakata et al., 1990). Details about the maximum-entropy calculations are given in Tables S8.1-S8.4 and S9.1-S9.4. The resolution $\sin\theta/\lambda$ was 0.55 \AA^{-1} for laboratory X-ray diffraction data. For synchrotron data three resolutions were chosen for comparison of MEM calculations: $\sin\theta/\lambda = 0.55 \text{ \AA}^{-1}$, $\sin\theta/\lambda = 0.65 \text{ \AA}^{-1}$, and $\sin\theta/\lambda = 0.93 \text{ \AA}^{-1}$. At highest diffraction angles the reflections are very broad and the correlation between the peak profile and background is very strong. Optimal values for the Lagrange multiplier λ were obtained by trial and error; an automated adjustment of λ during iterations was not possible due to an increase of the constraints values for several cycles of the iteration. Densities obtained in such a way would be unreliable and were not used. In the MEM calculations, the total number of electrons in the unit cell was given as a constant. The number of electrons for all missing atoms was included in the calculations.

Special attention was given to the value of the stopping criterion χ_{aim}^2 . Historically the MEM uses $\chi_{aim}^2 = 1$ as stopping criterion. Applying this stopping criterion to the present work resulted either in non-fitting of a significant amount of electron density or overfitting. Therefore, the stopping criterion was modified according to the procedure described in Hofmann et al. (2007) in order to avoid under- and overfitting of the electron density. The value of χ_{aim}^2 depended strongly on the occupancy of missing atoms, on the presence of other atoms in the hexagonal channel, on the type of the prior density (procrystal density or flat prior), on the type of constraints (F_{obs} , $F_{obs}+G$, $F_{LeBail}+G$) used for the MEM calculations, and on the resolution $\sin\theta/\lambda$ of X-ray diffraction data.

Section S2. Examples of Rietveld refinement and Le Bail fit.

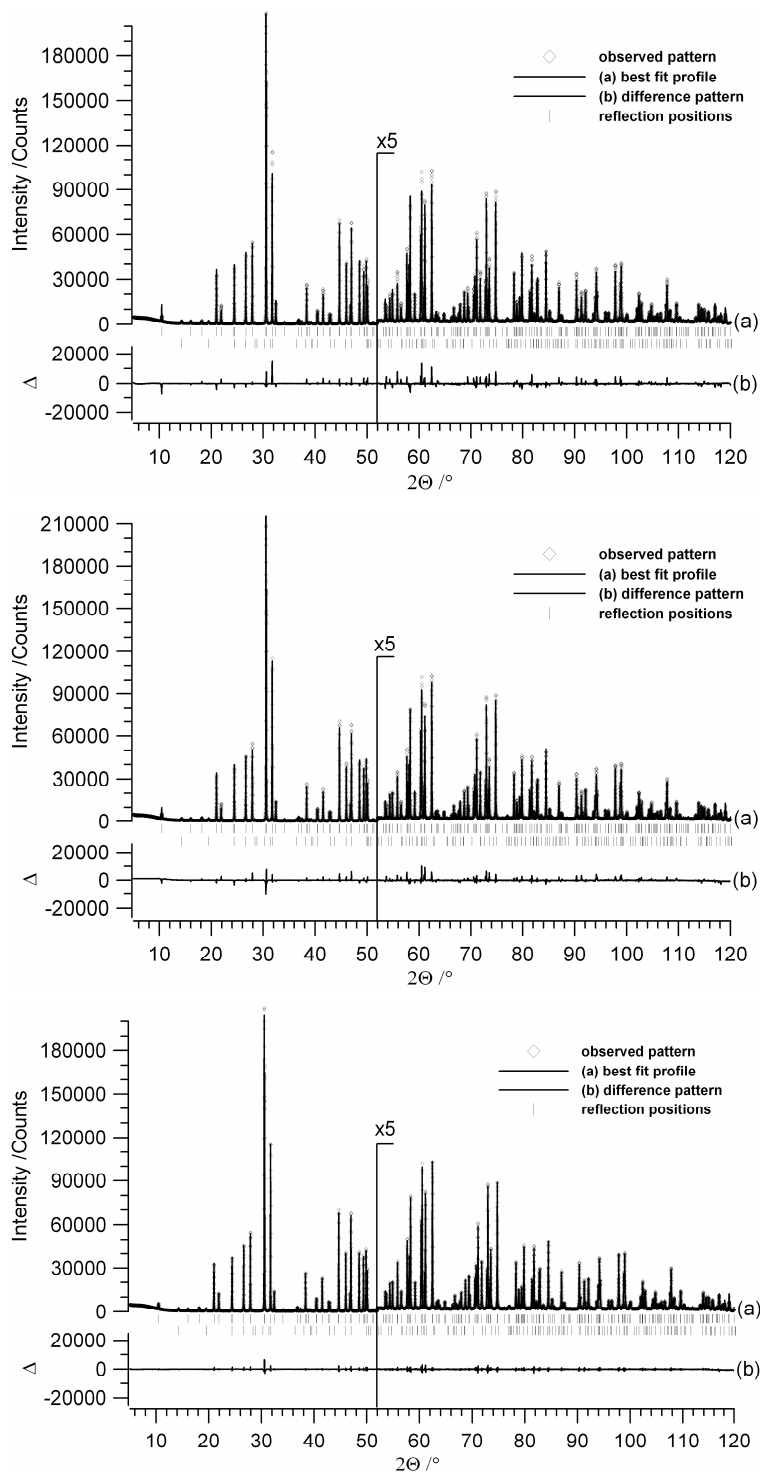


Fig. S2.1. Rietveld refinement of laboratory X-ray diffraction data of apatite $\text{Sr}_5(\text{PO}_4)_3\text{Cu}_{0.1}\text{OH}_{0.9-\delta}$ (sample SrA(0.1Cu-2), $\delta = 0.10$) without copper atoms (top), with included copper atoms (middle) and Le Bail fit (bottom). $\text{Sr}(\text{OH})_2 \cdot \text{H}_2\text{O}$ was refined as second phase (2%).

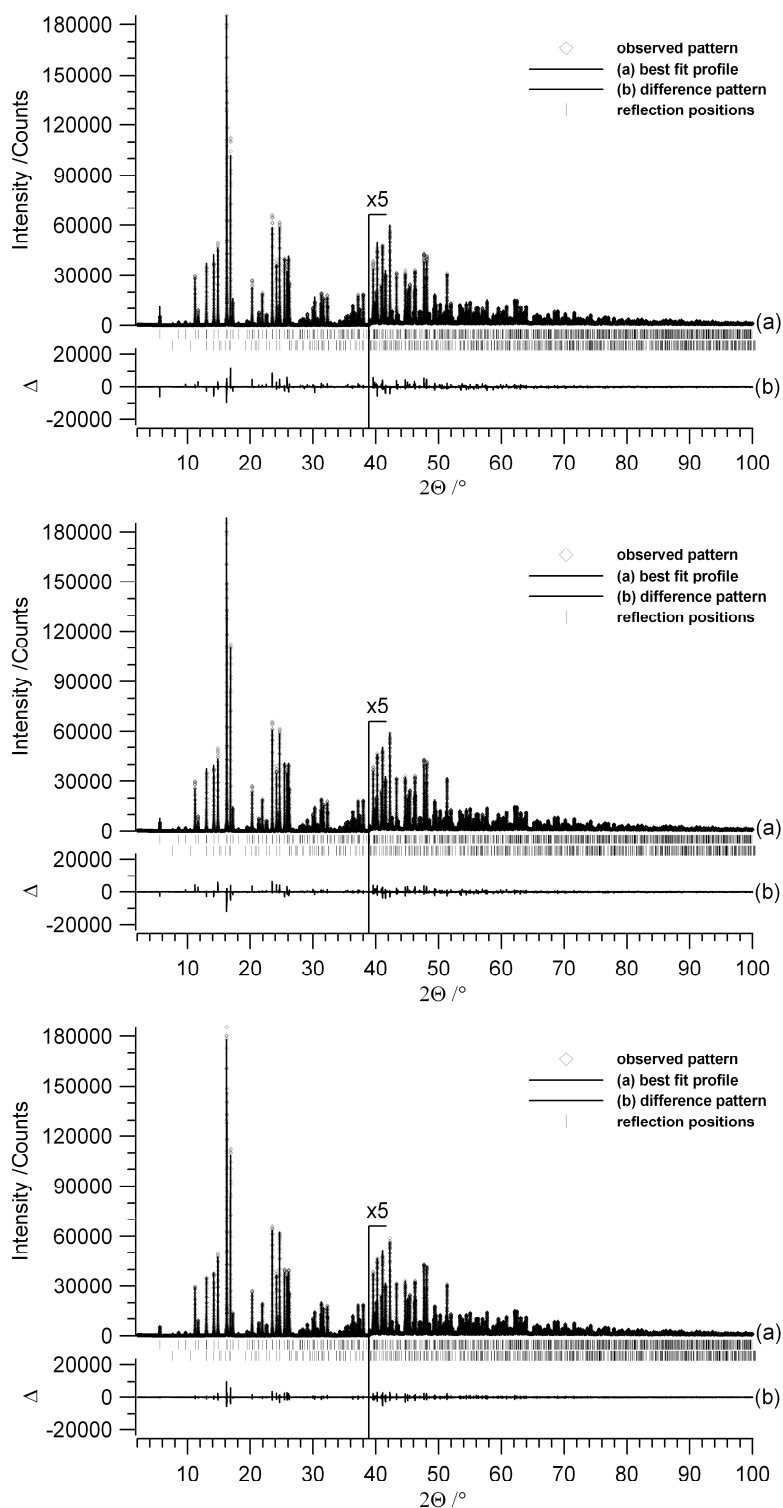


Fig. S2.2. Rietveld refinement of synchrotron X-ray diffraction data of apatite $\text{Sr}_5(\text{PO}_4)_3\text{Cu}_{0.1}\text{OH}_{0.9-\delta}$ (sample SrA(0.1Cu-2), $\delta = 0.10$) without copper atoms (top), with included copper atoms (middle) and Le Bail fit (bottom). $\text{Sr}(\text{OH})_2 \cdot \text{H}_2\text{O}$ was refined as second phase (2%).

Section S3. Localization of missing intercalated metal atoms from laboratory X-ray powder diffraction data

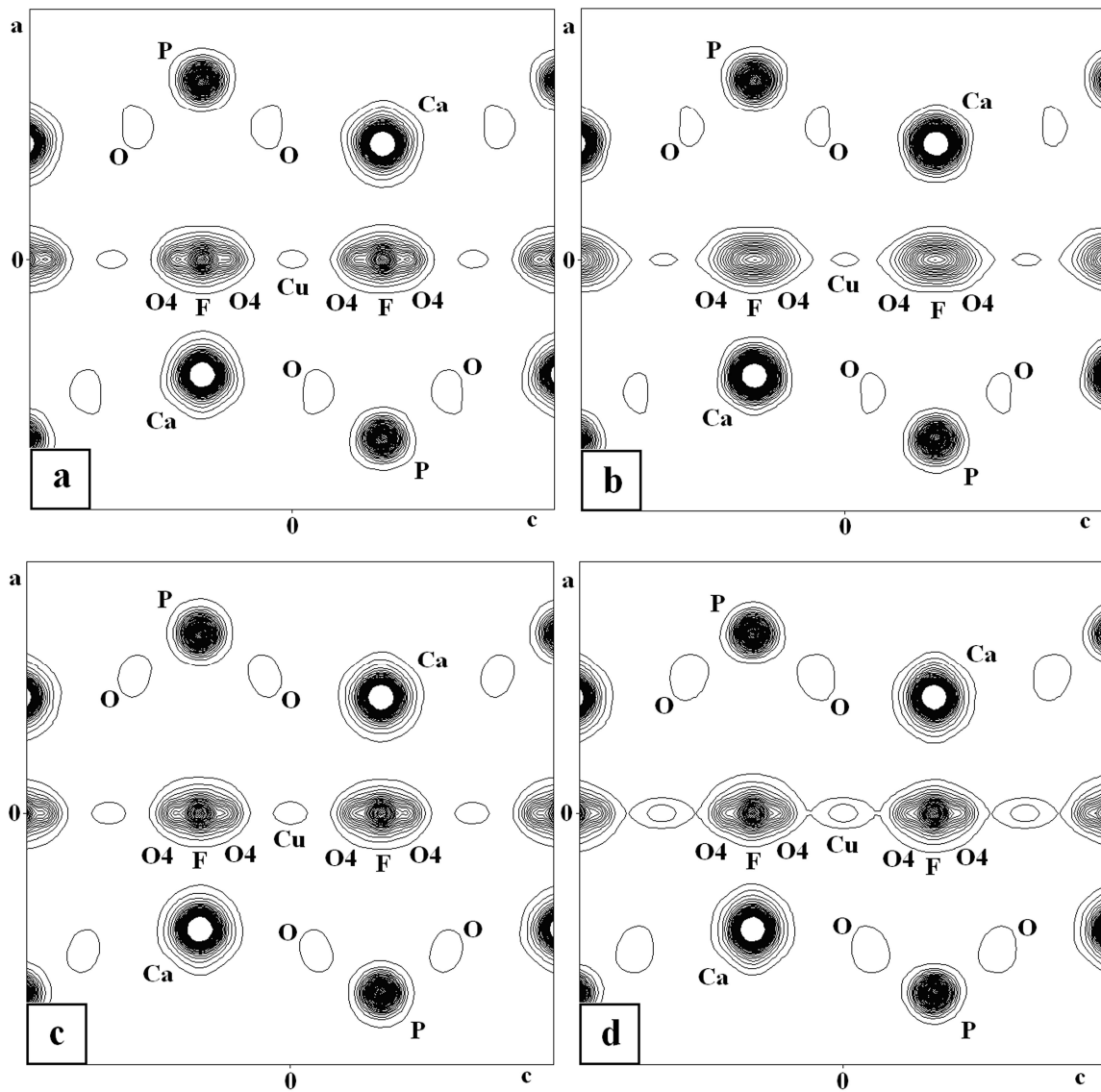


Fig. S3.1. Two-dimensional electron-density maps at $y=0$ of apatite $\text{Ca}_5(\text{PO}_4)_3\text{Cu}_{0.05}\text{O}_{0.5}\text{H}_{0.45-\delta}\text{F}_{0.5}$ (sample CaA(0.05Cu_0.5F)). Contour levels: from 1 to 50 $\text{e}/\text{\AA}^3$, step 1 $\text{e}/\text{\AA}^3$. High-resolution laboratory X-ray diffraction data.

- a) based on F_{obs} (with procrystal density for known atoms)
- b) based on F_{obs} (with flat prior)
- c) based on $F_{\text{obs}}+G$ (with procrystal density for known atoms)
- d) based on $F_{\text{LeBail}}+G$ (with procrystal density for known atoms)

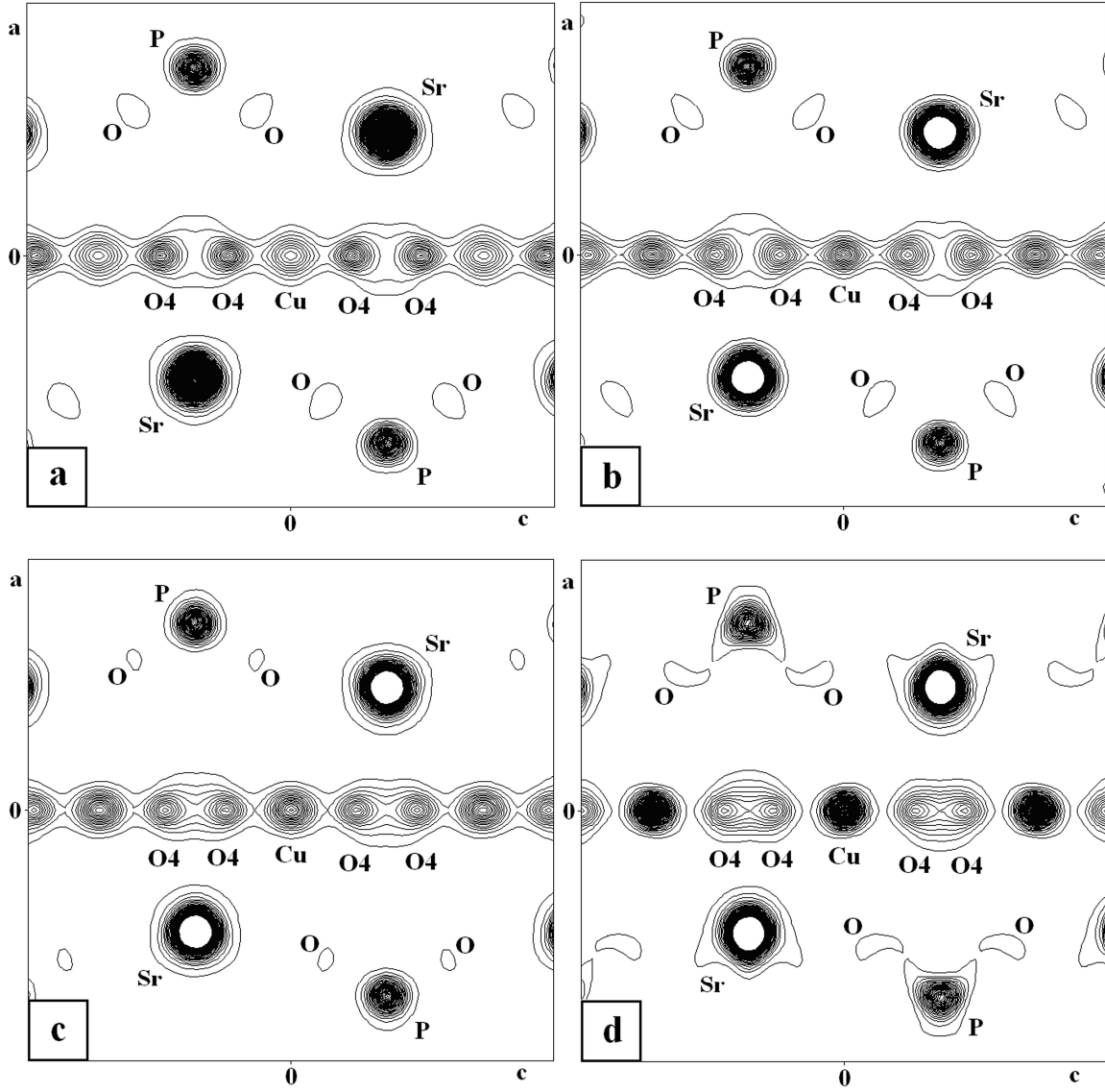


Fig. S3.2. Two-dimensional electron-density maps at $y=0$ of the apatite $\text{Sr}_5(\text{PO}_4)_3\text{Cu}_{0.25}\text{OH}_{0.75-\delta}$ (sample $\text{SrA}(0.25\text{Cu})$). Contour levels: from 1 to $50 \text{ e}/\text{\AA}^3$, step $1 \text{ e}/\text{\AA}^3$. High-resolution laboratory X-ray diffraction data.

- a) based on F_{obs} (with procrystal density for known atoms)
- b) based on F_{obs} (with flat prior)
- c) based on $F_{\text{obs}}+G$ (with procrystal density for known atoms)
- d) based on $F_{\text{LeBail}}+G$ (with procrystal density for known atoms)

Section S4. Localization of missing intercalated metal atoms from synchrotron X-ray powder diffraction data

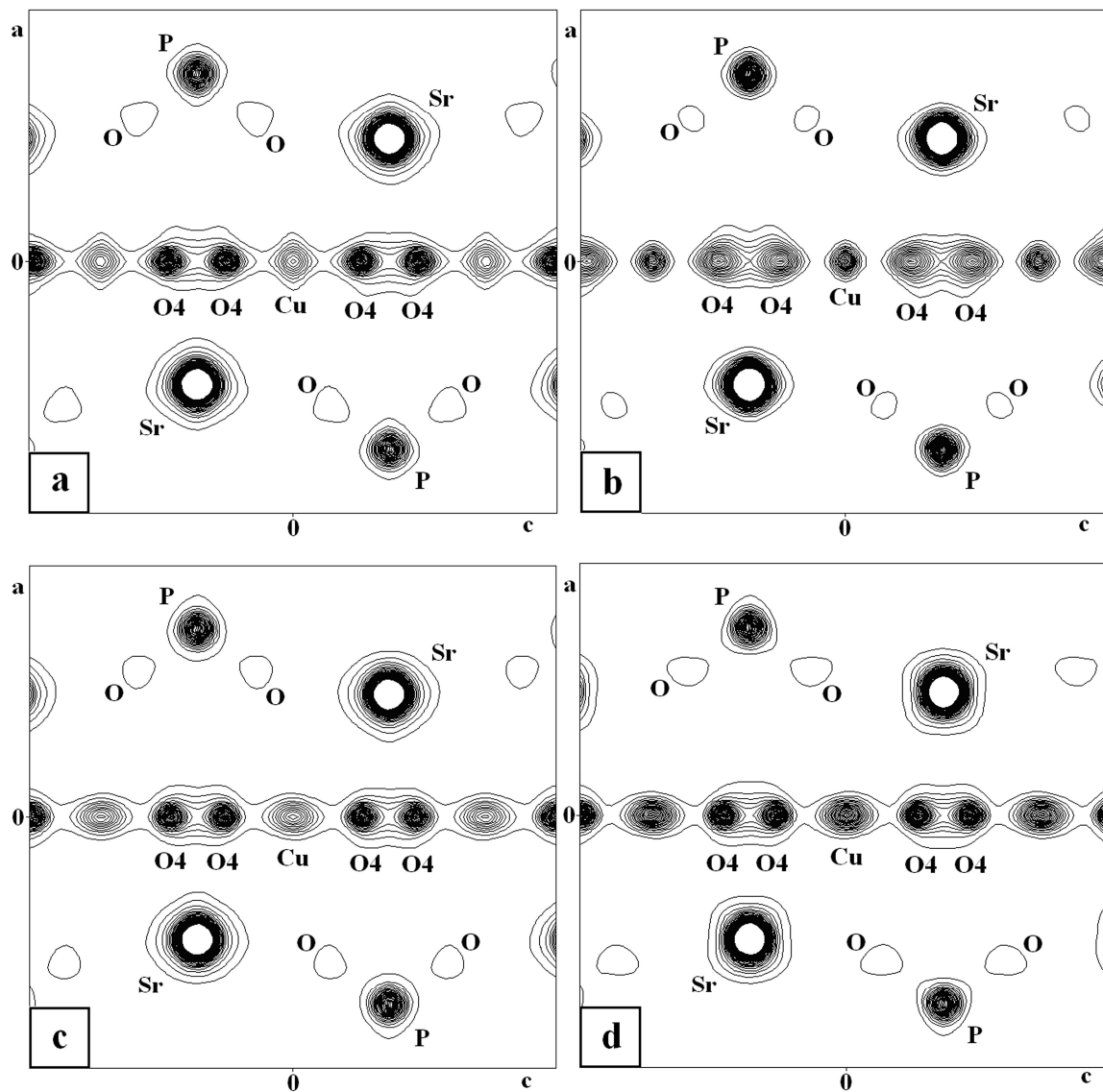


Fig. S4.1a. Two-dimensional electron-density maps at $y=0$ of apatite $\text{Sr}_5(\text{PO}_4)_3\text{Cu}_{0.1}\text{OH}_{0.9-\delta}$ (sample SrA(0.1Cu-1), $\delta = 0.038$). Contour levels: from 1 to $50 \text{ e}/\text{\AA}^3$, step $1 \text{ e}/\text{\AA}^3$. High-resolution synchrotron X-ray diffraction data with $\sin\theta/\lambda = 0.55$.

- a) based on F_{obs} (with procrystal density for known atoms)
- b) based on F_{obs} (with flat prior)
- c) based on $F_{\text{obs}}+G$ (with procrystal density for known atoms)
- d) based on $F_{\text{LeBail}}+G$ (with procrystal density for known atoms)

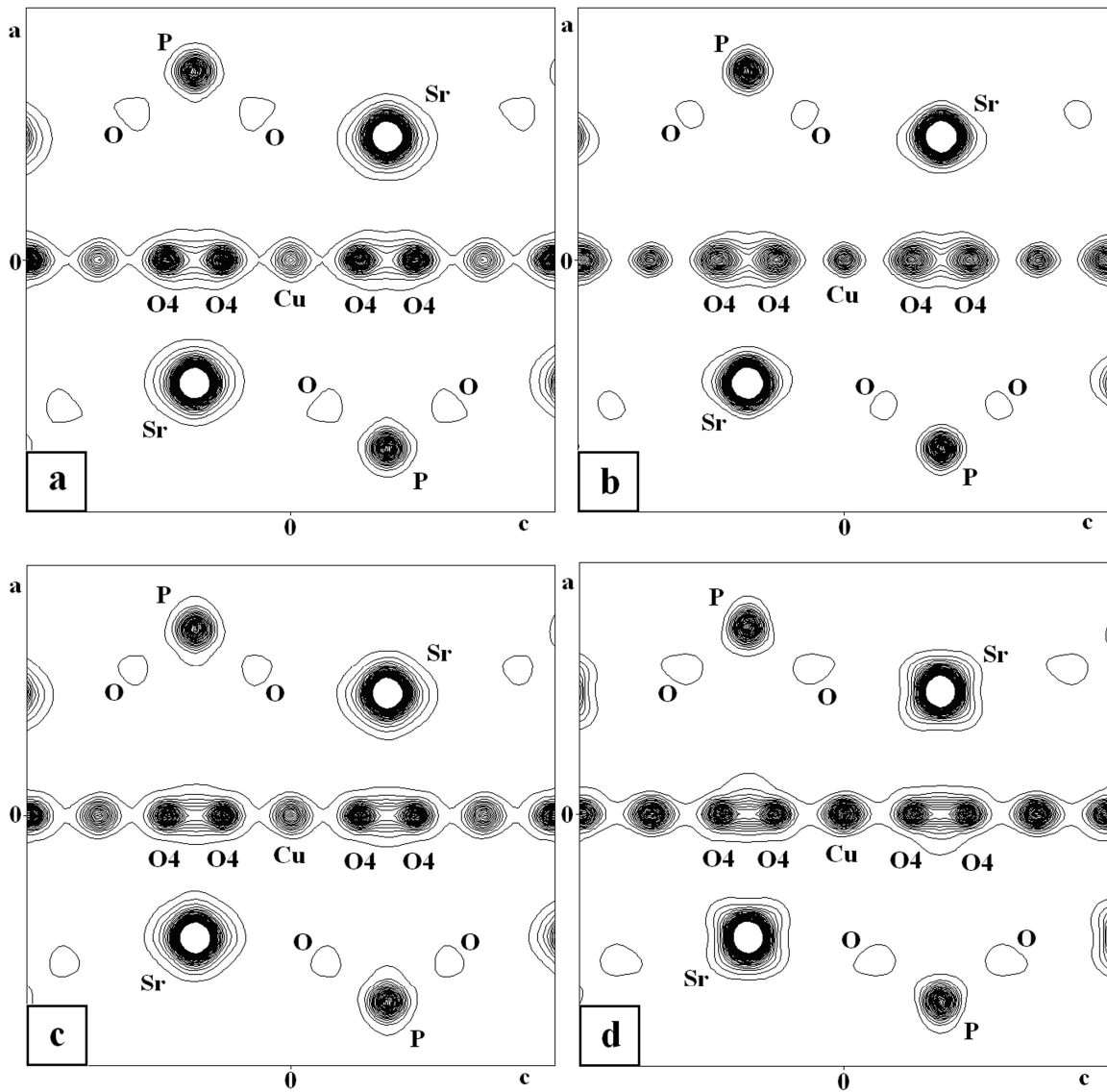


Fig. S4.1b. Two-dimensional electron-density maps at $y=0$ of apatite $\text{Sr}_5(\text{PO}_4)_3\text{Cu}_{0.1}\text{OH}_{0.9-\delta}$ (sample SrA(0.1Cu-1), $\delta = 0.038$). Contour levels: from 1 to 50 $\text{e}/\text{\AA}^3$, step 1 $\text{e}/\text{\AA}^3$. High-resolution synchrotron X-ray diffraction data with $\sin\theta/\lambda = 0.65$.

- a) based on F_{obs} (with procrystal density for known atoms)
- b) based on F_{obs} (with flat prior)
- c) based on $F_{\text{obs}}+G$ (with procrystal density for known atoms)
- d) based on $F_{\text{LeBail}}+G$ (with procrystal density for known atoms)

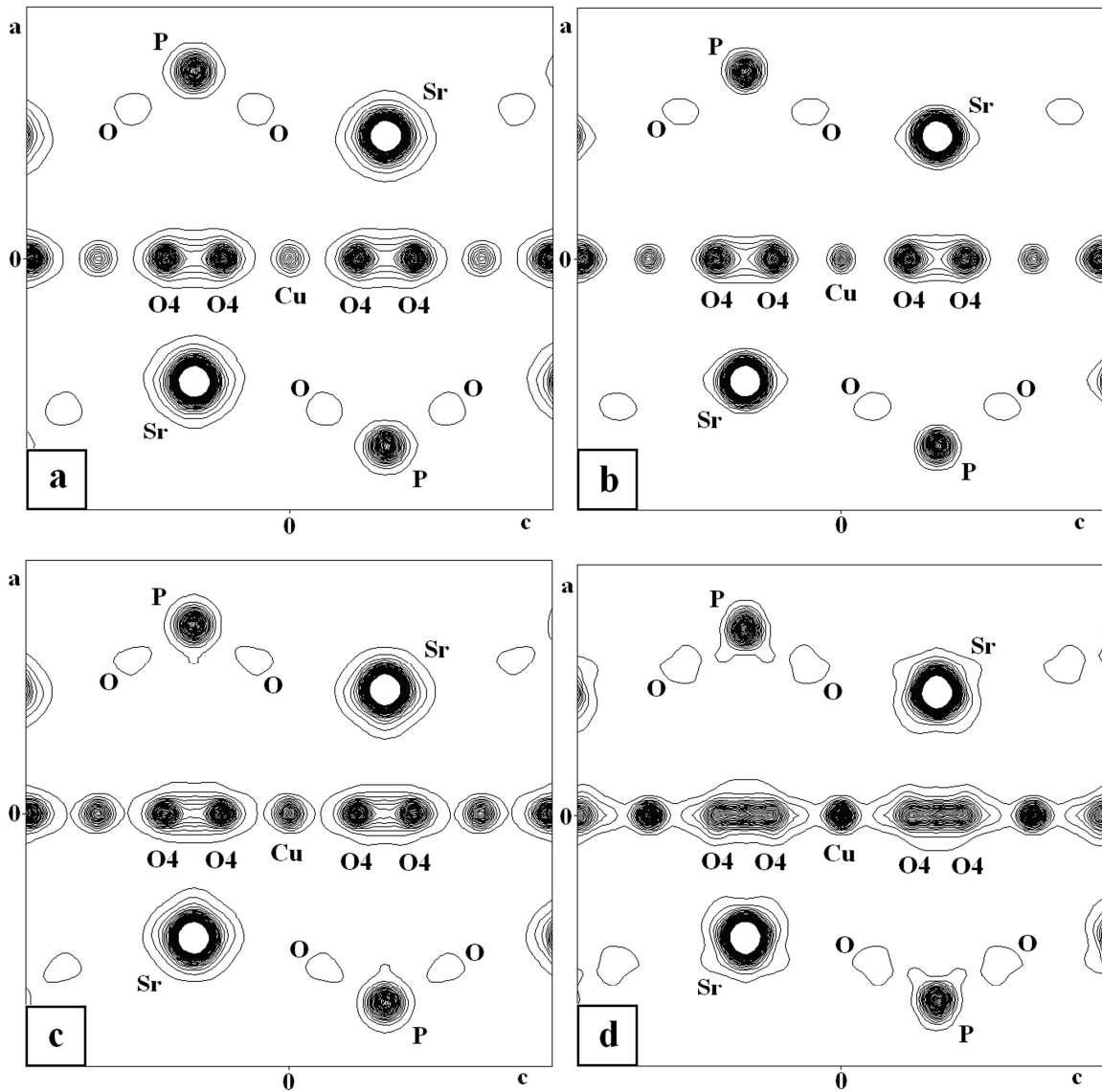


Fig. S4.1c. Two-dimensional electron-density maps at $y=0$ of apatite $\text{Sr}_5(\text{PO}_4)_3\text{Cu}_{0.1}\text{OH}_{0.9-\delta}$ (sample SrA(0.1Cu-1), $\delta = 0.038$). Contour levels: from 1 to $50 \text{ e}/\text{\AA}^3$, step $1 \text{ e}/\text{\AA}^3$. High-resolution synchrotron X-ray diffraction data with $\sin\theta/\lambda = 0.93$.

- a) based on F_{obs} (with procrystal density for known atoms)
- b) based on F_{obs} (with flat prior)
- c) based on $F_{\text{obs}}+G$ (with procrystal density for known atoms)
- d) based on $F_{\text{LeBail}}+G$ (with procrystal density for known atoms)

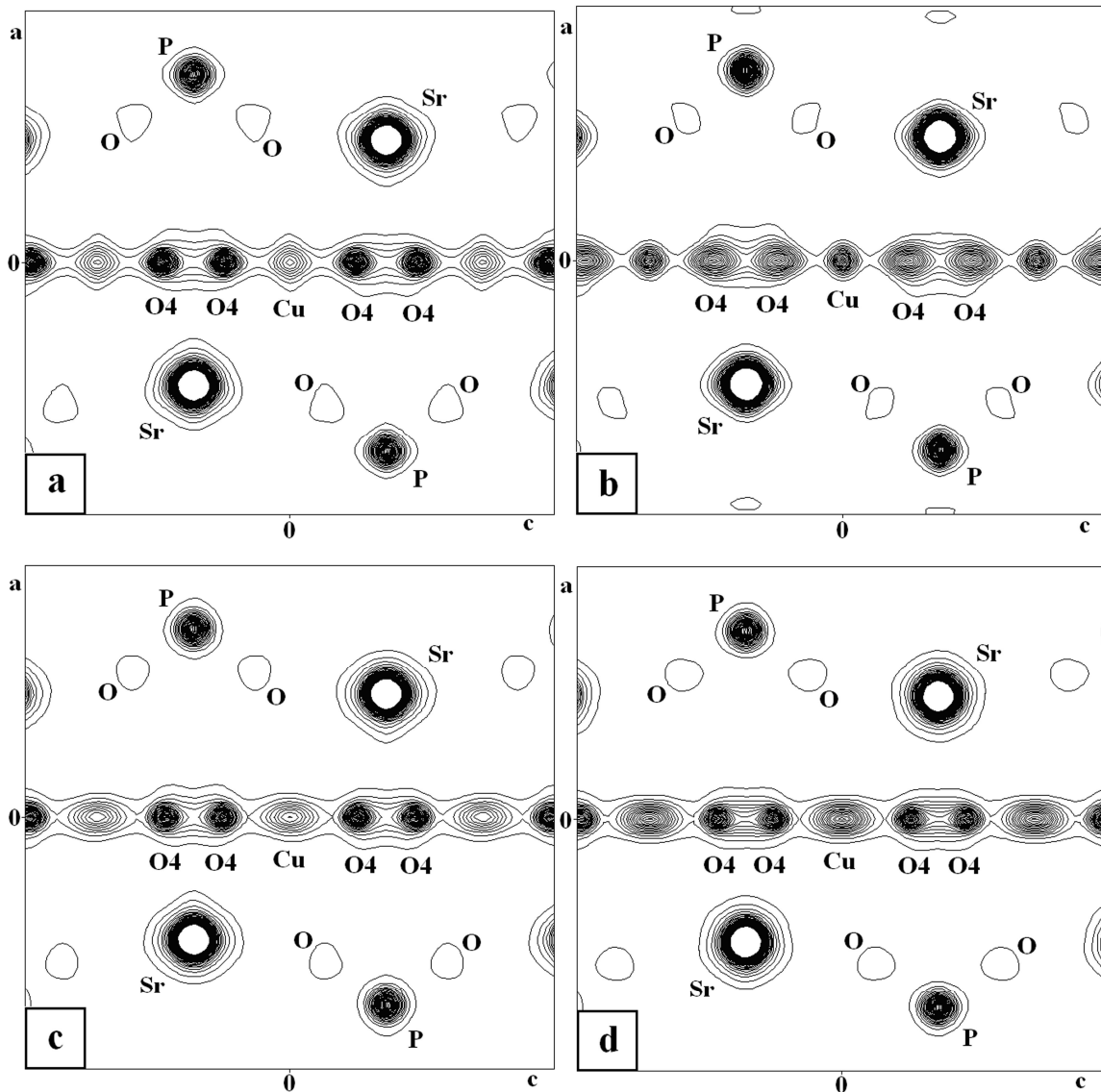


Fig. S4.2a. Two-dimensional electron-density maps at $y=0$ of apatite $\text{Sr}_5(\text{PO}_4)_3\text{Cu}_{0.1}\text{OH}_{0.9-\delta}$ (sample SrA(0.1Cu-3), $\delta = 0.26$). Contour levels: from 1 to 50 $\text{e}/\text{\AA}^3$, step 1 $\text{e}/\text{\AA}^3$. High-resolution synchrotron X-ray diffraction data with $\sin\theta/\lambda = 0.55$.

- a) based on F_{obs} (with procrystal density for known atoms)
- b) based on F_{obs} (with flat prior)
- c) based on $F_{\text{obs}}+G$ (with procrystal density for known atoms)
- d) based on $F_{\text{LeBail}}+G$ (with procrystal density for known atoms)

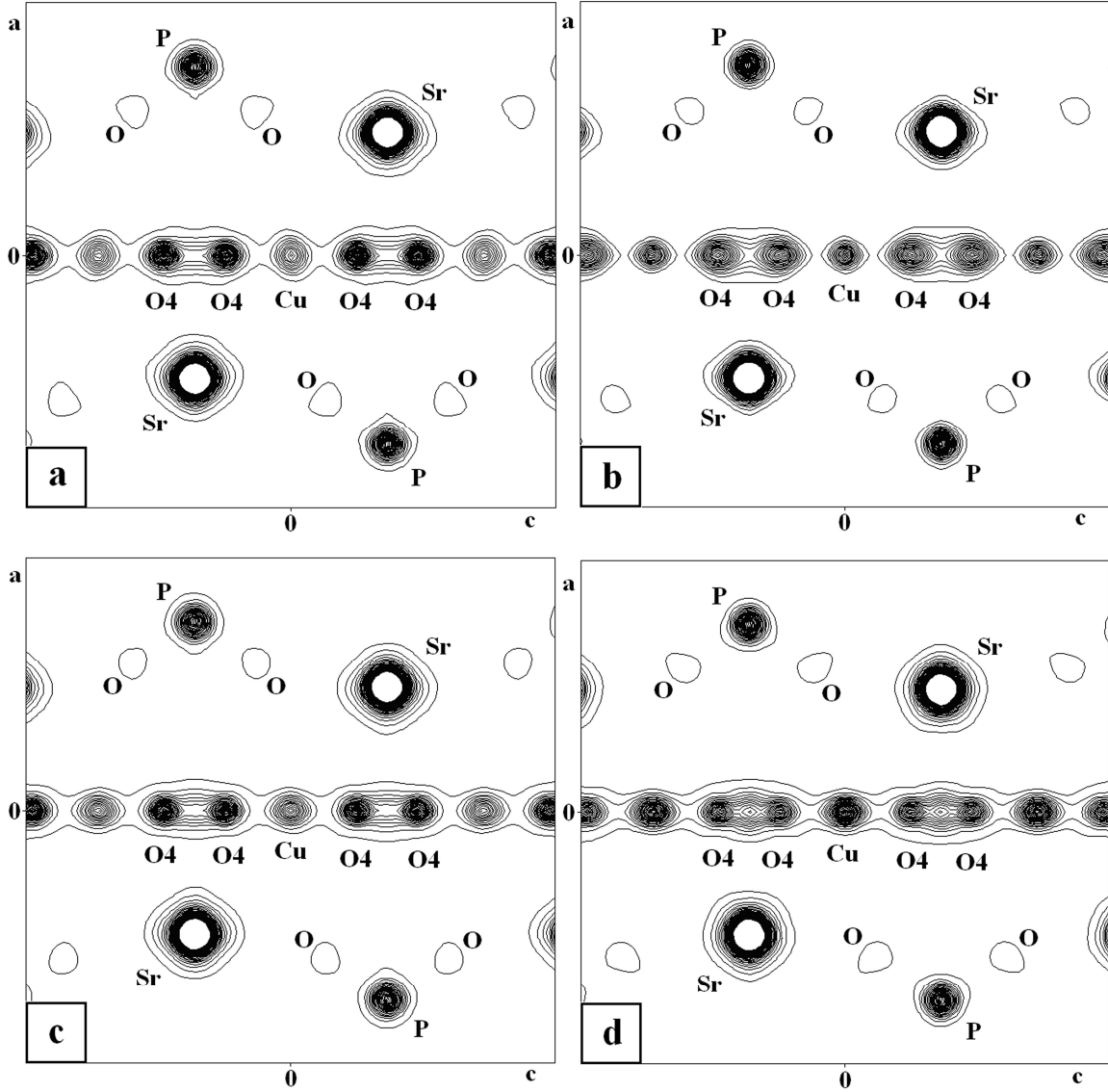


Fig. S4.2b. Two-dimensional electron-density maps at $y=0$ of apatite $\text{Sr}_5(\text{PO}_4)_3\text{Cu}_{0.1}\text{OH}_{0.9-\delta}$ (sample SrA(0.1Cu-3), $\delta = 0.26$). Contour levels: from 1 to 50 $\text{e}/\text{\AA}^3$, step 1 $\text{e}/\text{\AA}^3$. High-resolution synchrotron X-ray diffraction data with $\sin\theta/\lambda = 0.65$.

- a) based on F_{obs} (with procrystal density for known atoms)
- b) based on F_{obs} (with flat prior)
- c) based on $F_{\text{obs}}+G$ (with procrystal density for known atoms)
- d) based on $F_{\text{LeBail}}+G$ (with procrystal density for known atoms)

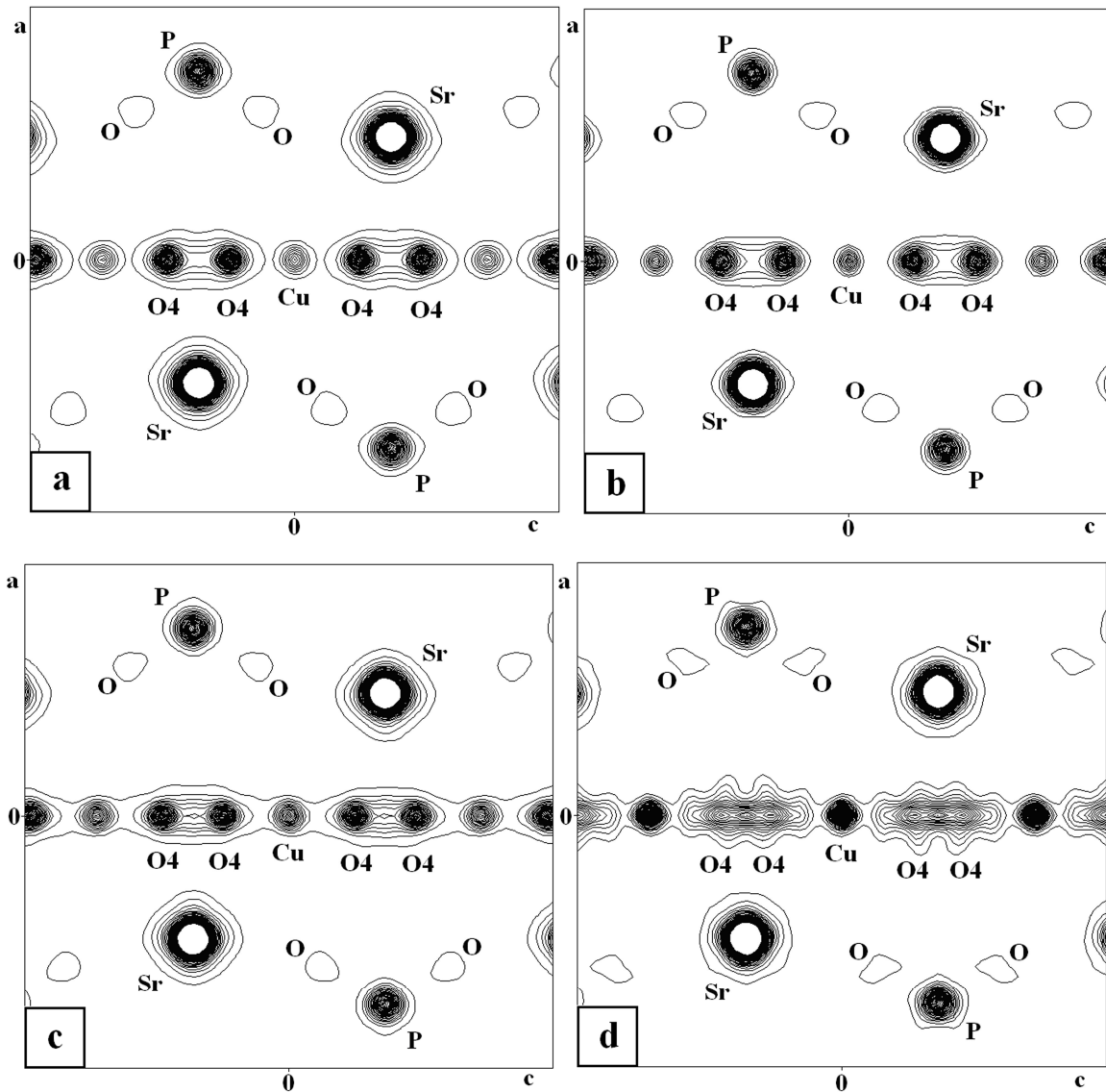


Fig. S4.2c. Two-dimensional electron-density maps at $y=0$ of apatite $\text{Sr}_5(\text{PO}_4)_3\text{Cu}_{0.1}\text{OH}_{0.9-\delta}$ (sample SrA(0.1Cu-3), $\delta = 0.26$). Contour levels: from 1 to 50 $\text{e}/\text{\AA}^3$, step 1 $\text{e}/\text{\AA}^3$. High-resolution synchrotron X-ray diffraction data with $\sin\theta/\lambda = 0.93$.

- a) based on F_{obs} (with procrystal density for known atoms)
- b) based on F_{obs} (with flat prior)
- c) based on $F_{\text{obs}}+G$ (with procrystal density for known atoms)
- d) based on $F_{\text{LeBail}}+G$ (with procrystal density for known atoms)

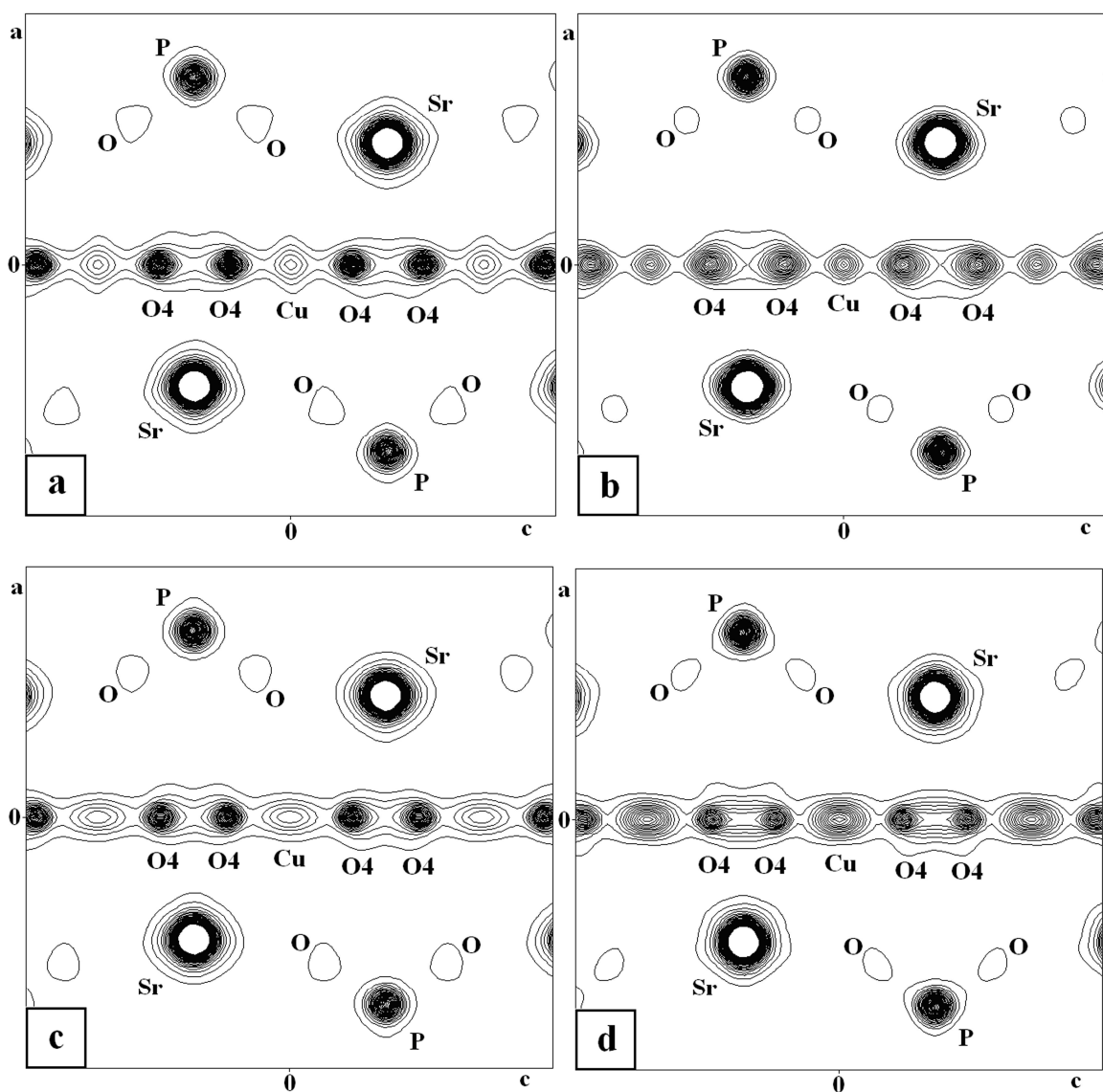


Fig. S4.3a. Two-dimensional electron-density maps at $y=0$ of apatite $\text{Sr}_5(\text{PO}_4)_3\text{Cu}_{0.1}\text{OH}_{0.9-\delta}$ (sample SrA(0.1Cu-4), $\delta > 0.26$). Contour levels: from 1 to 50 $\text{e}/\text{\AA}^3$, step 1 $\text{e}/\text{\AA}^3$. High-resolution synchrotron X-ray diffraction data with $\sin\theta/\lambda = 0.55$.

- a) based on F_{obs} (with procrystal density for known atoms)
- b) based on F_{obs} (with flat prior)
- c) based on $F_{\text{obs}}+G$ (with procrystal density for known atoms)
- d) based on $F_{\text{LeBail}}+G$ (with procrystal density for known atoms)

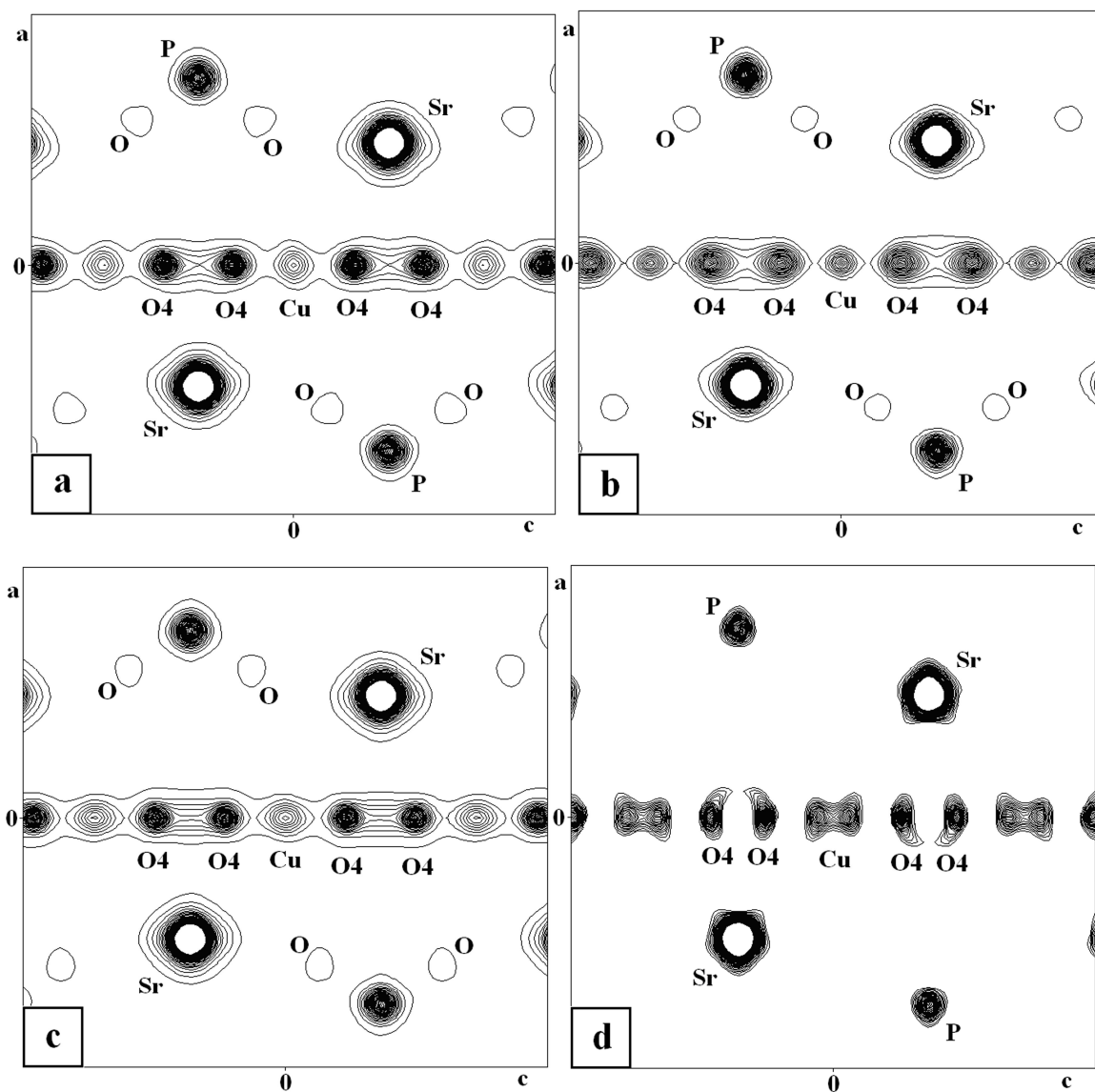


Fig. S4.3b. Two-dimensional electron-density maps at $y=0$ of apatite $\text{Sr}_5(\text{PO}_4)_3\text{Cu}_{0.1}\text{OH}_{0.9-\delta}$ (sample SrA(0.1Cu-4), $\delta > 0.26$). Contour levels: from 1 to 50 (from 3 to 50 – case d) $\text{e}/\text{\AA}^3$, step $1 \text{ e}/\text{\AA}^3$. High-resolution synchrotron X-ray diffraction data with $\sin\theta/\lambda = 0.65$.

- a) based on F_{obs} (with procrystal density for known atoms)
- b) based on F_{obs} (with flat prior)
- c) based on $F_{\text{obs}}+G$ (with procrystal density for known atoms)
- d) based on $F_{\text{LeBail}}+G$ (with procrystal density for known atoms)

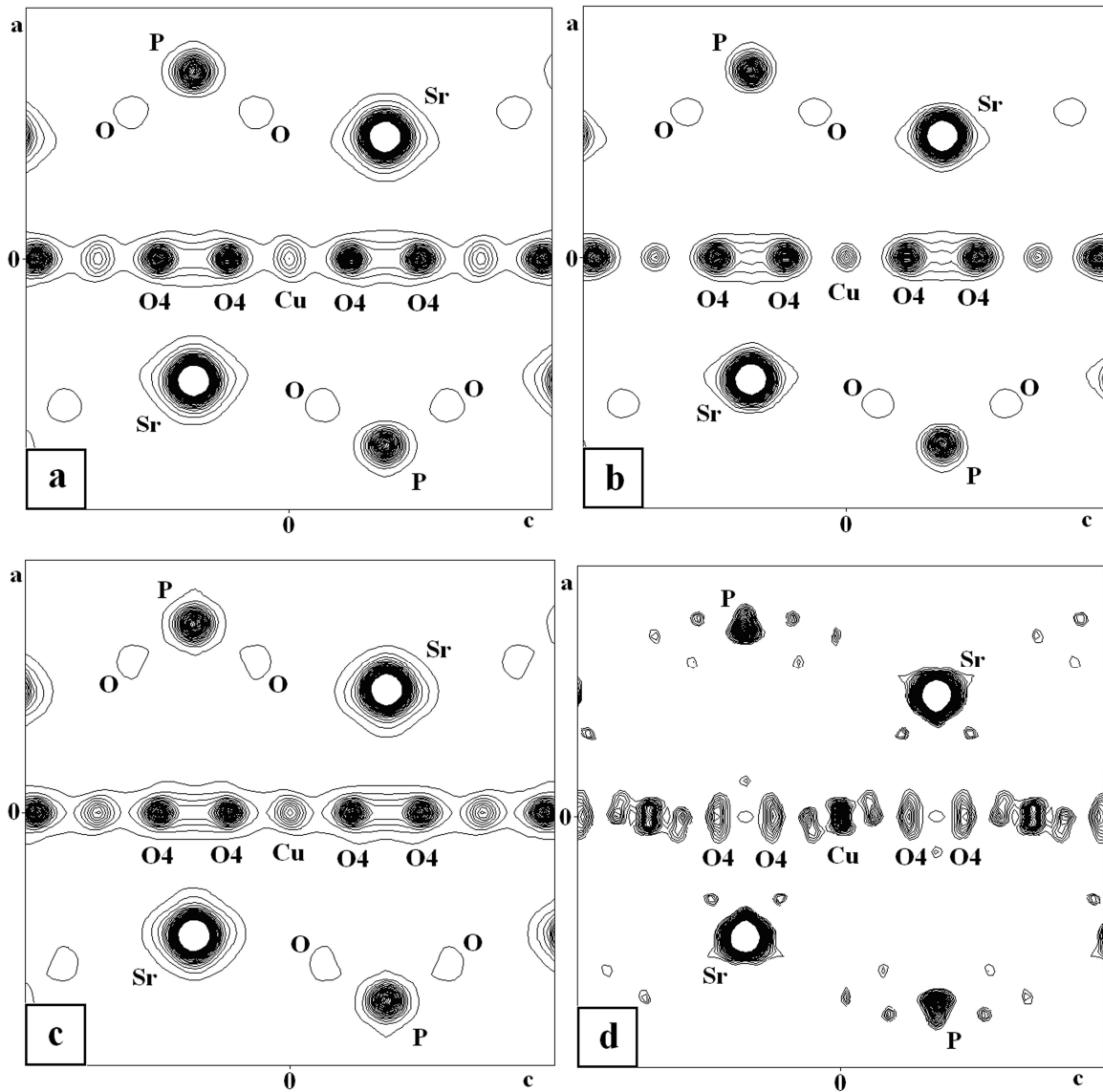


Fig. S4.3c. Two-dimensional electron-density maps at $y=0$ of apatite $\text{Sr}_5(\text{PO}_4)_3\text{Cu}_{0.1}\text{OH}_{0.9-\delta}$ (sample SrA(0.1Cu-4), $\delta > 0.26$). Contour levels: from 1 to 50 (from 3 to 50 – case d) $\text{e}/\text{\AA}^3$, step $1 \text{ e}/\text{\AA}^3$. High-resolution synchrotron X-ray diffraction data with $\sin\theta/\lambda = 0.93$.

- a) based on F_{obs} (with procrystal density for known atoms)
- b) based on F_{obs} (with flat prior)
- c) based on $F_{\text{obs}}+G$ (with procrystal density for known atoms)
- d) based on $F_{\text{LeBail}}+G$ (with procrystal density for known atoms)

Section S5. Determination of the electron density distribution from synchrotron X-ray powder diffraction data

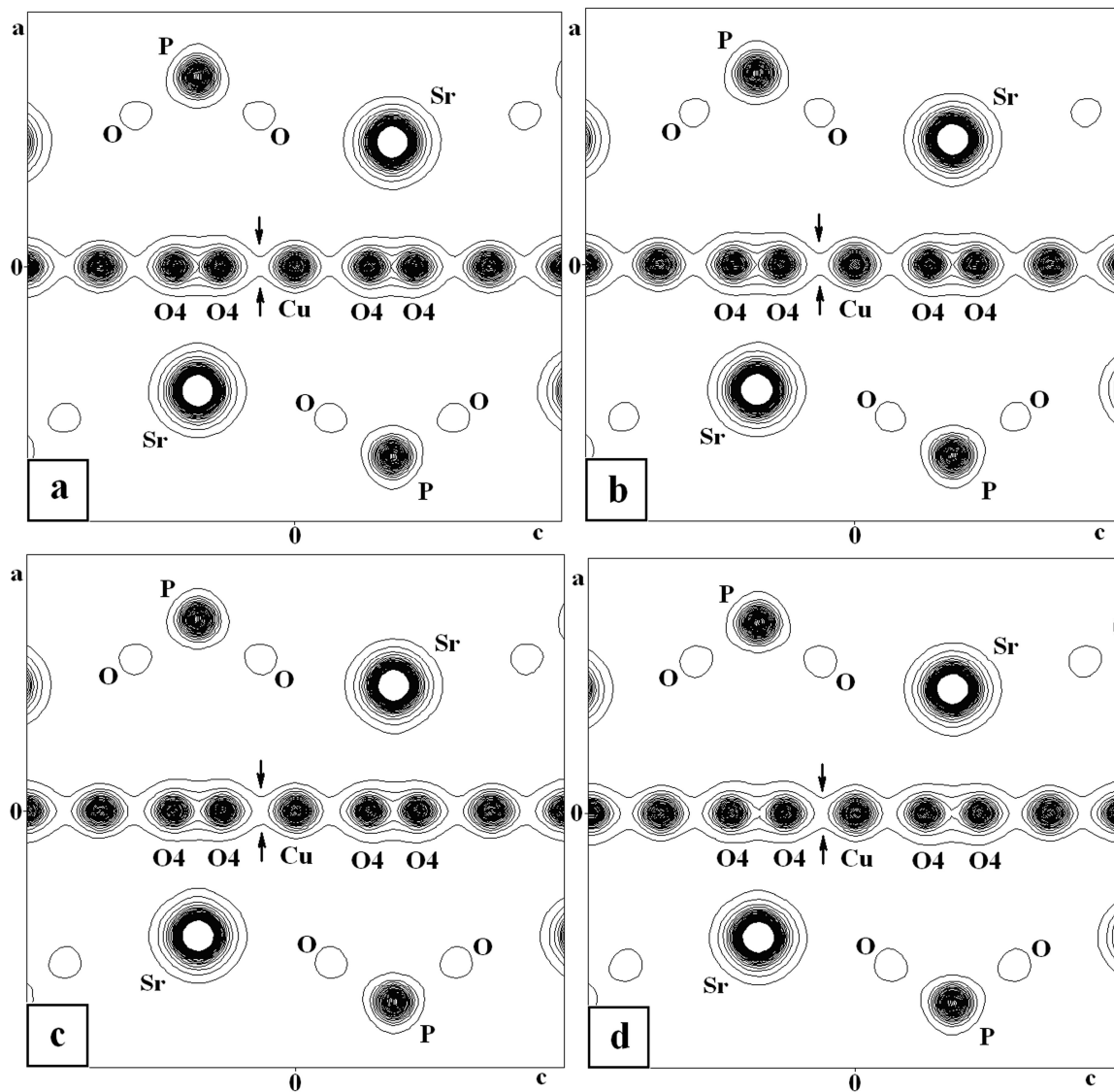


Fig. S5.1a. Two-dimensional electron-density maps based on $F_{\text{obs}}+G$ (with procrystal density for complete structure) at $y=0$ of apatites $\text{Sr}_5(\text{PO}_4)_3\text{Cu}_{0.1}\text{OH}_{0.9-\delta}$ with different content of peroxide and copper ions in higher oxidation state. Contour levels: from 1 to $50 \text{ e}/\text{\AA}^3$, step $1 \text{ e}/\text{\AA}^3$. High-resolution synchrotron X-ray diffraction data with $\sin\theta/\lambda = 0.55$. Arrows show the distortion of the electron density near the copper atom.

- a) $\text{Sr}_5(\text{PO}_4)_3\text{Cu}_{0.1}\text{OH}_{0.9-\delta}$ (sample SrA(0.1Cu-1), $\delta = 0.038$)
- b) $\text{Sr}_5(\text{PO}_4)_3\text{Cu}_{0.1}\text{OH}_{0.9-\delta}$ (sample SrA(0.1Cu-2), $\delta = 0.10$)
- c) $\text{Sr}_5(\text{PO}_4)_3\text{Cu}_{0.1}\text{OH}_{0.9-\delta}$ (sample SrA(0.1Cu-3), $\delta = 0.26$)
- d) $\text{Sr}_5(\text{PO}_4)_3\text{Cu}_{0.1}\text{OH}_{0.9-\delta}$ (sample SrA(0.1Cu-4), $\delta > 0.26$)

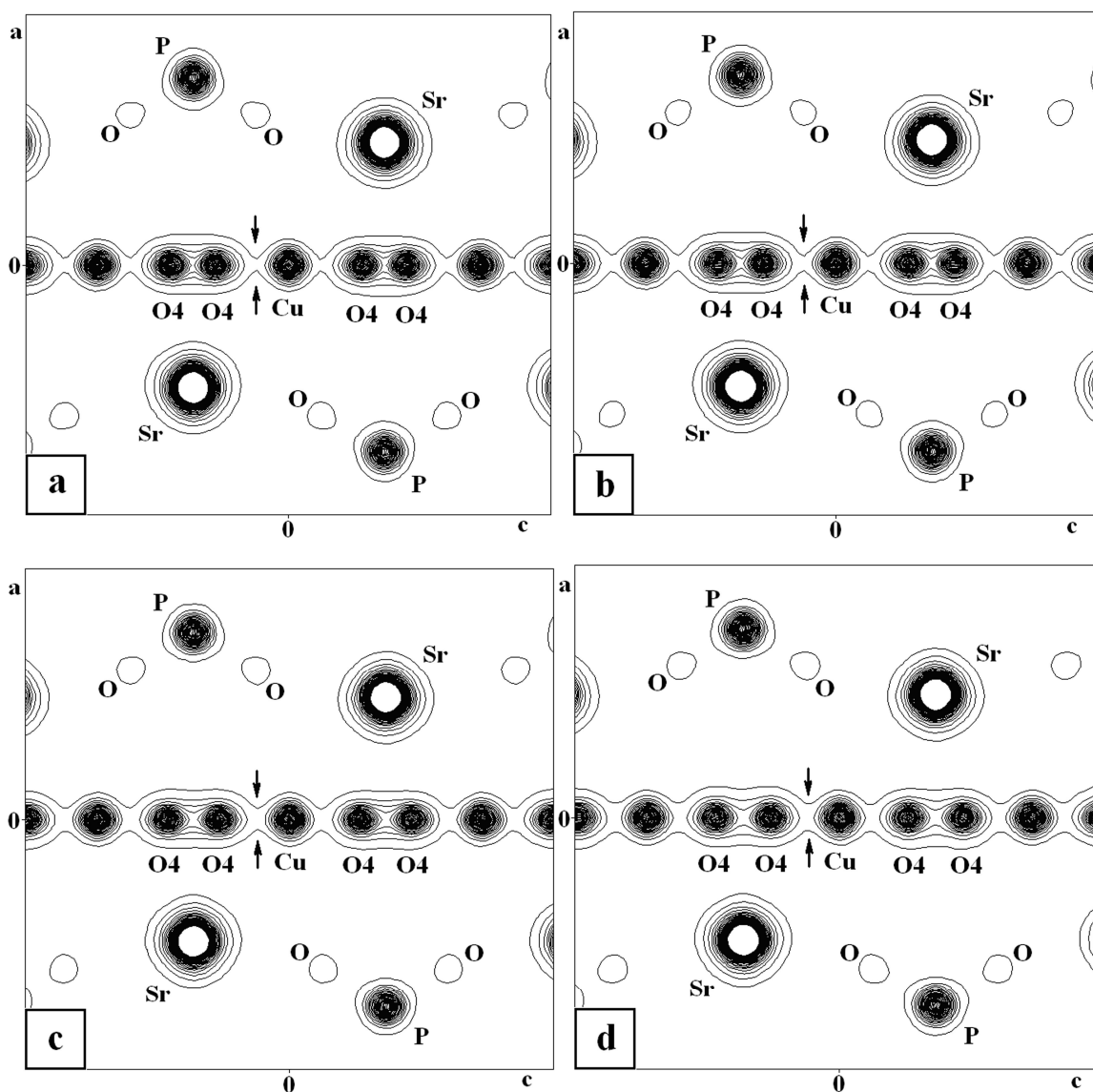


Fig. S5.1b. Two-dimensional electron-density maps based on $F_{\text{obs}}+G$ (with procrystal density for complete structure) at $y=0$ of apatites $\text{Sr}_5(\text{PO}_4)_3\text{Cu}_{0.1}\text{OH}_{0.9-\delta}$ with different content of peroxide and copper ions in higher oxidation state. Contour levels: from 1 to $50 \text{ e}/\text{\AA}^3$, step $1 \text{ e}/\text{\AA}^3$. High-resolution synchrotron X-ray diffraction data with $\sin\theta/\lambda = 0.65$. Arrows show the distortion of the electron density near the copper atom.

- a) $\text{Sr}_5(\text{PO}_4)_3\text{Cu}_{0.1}\text{OH}_{0.9-\delta}$ (sample SrA(0.1Cu-1), $\delta = 0.038$)
- b) $\text{Sr}_5(\text{PO}_4)_3\text{Cu}_{0.1}\text{OH}_{0.9-\delta}$ (sample SrA(0.1Cu-2), $\delta = 0.10$)
- c) $\text{Sr}_5(\text{PO}_4)_3\text{Cu}_{0.1}\text{OH}_{0.9-\delta}$ (sample SrA(0.1Cu-3), $\delta = 0.26$)
- d) $\text{Sr}_5(\text{PO}_4)_3\text{Cu}_{0.1}\text{OH}_{0.9-\delta}$ (sample SrA(0.1Cu-4), $\delta > 0.26$)

Section S6.

Table S6.1. Crystallographic and refinement data (Rietveld refinement and Le Bail fit of incomplete crystal structures without intercalated metal atoms) for hydroxyapatites (space group $P6_3/m$ (176)) with different intercalated metal atoms from laboratory X-ray powder diffraction data (R_{Br} , R_p , R_{wp} and $GooF$ as defined in Topas).

Sample	SrA(0.25Cu)	CaA(0.1Cu)	SrA(0.2Ni)	SrA(0.15Zn)
Molecular formula	$\text{Sr}_5(\text{PO}_4)_3\text{Cu}_{0.25}\text{OH}_{0.75-\delta}$	$\text{Ca}_5(\text{PO}_4)_3\text{Cu}_{0.1}\text{OH}_{0.9-\delta}$	$\text{Sr}_5(\text{PO}_4)_3\text{Ni}_{0.2}\text{OH}_{0.8-\delta}$	$\text{Sr}_5(\text{PO}_4)_3\text{Zn}_{0.15}\text{OH}_{0.85-\delta}$
Z	2	2	2	2
$a / \text{\AA}$	9.7780(3)	9.4220(2)	9.7743(2)	9.7531(2)
$c / \text{\AA}$	7.2942(2)	6.8871(2)	7.2977(2)	7.3088(2)
R_{Br} , % (Rietveld)	11.16	9.64	4.88	4.91
R_p , % (Rietveld)	11.11	10.60	5.74	5.58
R_{wp} , % (Rietveld)	17.71	15.84	7.63	7.62
$GooF$ (Rietveld)	6.95	3.48	1.19	1.81
R_p , % (Le Bail)	4.42	5.89	3.79	3.53
R_{wp} , % (Le Bail)	6.94	7.95	5.33	4.74
$GooF$ (Le Bail)	2.72	1.75	0.83	1.13
Temperature (K)	293	293	293	293
Wavelength (\AA)	1.540596	1.540596	1.540596	1.540596
2θ – range ($^\circ$)	10 – 120	10 – 120	15 – 100	15 – 100
Step width ($^\circ 2\theta$)	0.0079	0.0079	0.01	0.01

Sample	CaA(0.1Cu_0.5F)	CaA(0.05Cu_0.5F)	CaA(0.02Cu_0.5F)	CaA(0.01Cu_0.5F)
Molecular formula	$\text{Ca}_5(\text{PO}_4)_3\text{Cu}_{0.1}\text{O}_{0.5}\text{H}_{0.4-\delta}\text{F}_{0.5}$	$\text{Ca}_5(\text{PO}_4)_3\text{Cu}_{0.05}\text{O}_{0.5}\text{H}_{0.45-\delta}\text{F}_{0.5}$	$\text{Ca}_5(\text{PO}_4)_3\text{Cu}_{0.02}\text{O}_{0.5}\text{H}_{0.48-\delta}\text{F}_{0.5}$	$\text{Ca}_5(\text{PO}_4)_3\text{Cu}_{0.01}\text{O}_{0.5}\text{H}_{0.49-\delta}\text{F}_{0.5}$
Z	2	2	2	2
$a / \text{\AA}$	9.3977(2)	9.3954(2)	9.3941(2)	9.3932(2)
$c / \text{\AA}$	6.8930(2)	6.8890(2)	6.8855(2)	6.8846(2)
R_{Br} , % (Rietveld)	8.97	7.17	5.42	4.48
R_p , % (Rietveld)	9.76	8.46	7.62	6.10
R_{wp} , % (Rietveld)	15.56	12.59	11.05	8.62
$GooF$ (Rietveld)	3.32	2.59	2.41	2.09
R_p , % (Le Bail)	4.83	5.18	4.96	4.40
R_{wp} , % (Le Bail)	6.54	7.05	7.11	6.10
$GooF$ (Le Bail)	1.40	1.45	1.55	1.48
Temperature (K)	293	293	293	293
Wavelength (\AA)	1.540596	1.540596	1.540596	1.540596
2θ – range ($^\circ$)	10 – 120	10 – 120	10 – 120	10 – 120
Step width ($^\circ 2\theta$)	0.0079	0.0079	0.0079	0.0079

Sample	SrA(0.1Cu-1)	SrA(0.1Cu-3)	SrA(0.1Cu-4)
Molecular formula	$\text{Sr}_5(\text{PO}_4)_3\text{Cu}_{0.1}\text{OH}_{0.9-\delta}$	$\text{Sr}_5(\text{PO}_4)_3\text{Cu}_{0.1}\text{OH}_{0.9-\delta}$	$\text{Sr}_5(\text{PO}_4)_3\text{Cu}_{0.1}\text{OH}_{0.9-\delta}$
<i>Z</i>	2	2	2
<i>a</i> / Å	9.7689(3)	9.7599(3)	9.7559(3)
<i>c</i> / Å	7.2849(3)	7.2788(3)	7.2771(3)
<i>R</i> _{Br} , % (Rietveld)	5.19	5.03	6.34
<i>R</i> _p , % (Rietveld)	7.03	6.26	7.61
<i>R</i> _w <i>p</i> , % (Rietveld)	11.01	9.90	12.59
<i>GooF</i> (Rietveld)	4.92	4.21	5.85
<i>R</i> _p , % (Le Bail)	4.58	3.09	3.10
<i>R</i> _w <i>p</i> , % (Le Bail)	7.54	4.93	4.43
<i>GooF</i> (Le Bail)	3.37	2.10	2.06
Temperature (K)	293	293	293
Wavelength (Å)	1.540596	1.540596	1.540596
2θ – range (°)	10 – 120	10 – 120	10 – 120
Step width (° 2θ)	0.0079	0.0079	0.0079

Table S6.2. Crystallographic and refinement data (Rietveld refinement and Le Bail fit of incomplete crystal structures without intercalated metal atoms) for hydroxyapatites SrA(0.1Cu-1), SrA(0.1Cu-2), SrA(0.1Cu-3), SrA(0.1Cu-4) from synchrotron X-ray powder diffraction data (*R*_{Br}, *R*_p, *R*_w*p* and *GooF* as defined in Topas).

Sample	SrA(0.1Cu-1)	SrA(0.1Cu-3)	SrA(0.1Cu-4)
Molecular formula	$\text{Sr}_5(\text{PO}_4)_3\text{Cu}_{0.1}\text{OH}_{0.9-\delta}$	$\text{Sr}_5(\text{PO}_4)_3\text{Cu}_{0.1}\text{OH}_{0.9-\delta}$	$\text{Sr}_5(\text{PO}_4)_3\text{Cu}_{0.1}\text{OH}_{0.9-\delta}$
<i>Z</i>	2	2	2
<i>a</i> / Å	9.7696(3)	9.7626(3)	9.7584(3)
<i>c</i> / Å	7.2855(3)	7.2821(3)	7.2782(3)
<i>R</i> _{Br} , % (Rietveld)	5.76	5.73	4.78
<i>R</i> _p , % (Rietveld)	8.07	6.57	6.20
<i>R</i> _w <i>p</i> , % (Rietveld)	11.12	9.61	9.07
<i>GooF</i> (Rietveld)	3.24	3.24	2.69
<i>R</i> _p , % (Le Bail)	6.18	4.04	3.78
<i>R</i> _w <i>p</i> , % (Le Bail)	8.01	5.39	5.01
<i>GooF</i> (Le Bail)	2.33	1.81	1.49
Temperature (K)	293	293	293
Wavelength (Å)	0.8264	0.8264	0.8264
2θ – range (°)	2 – 100	2 – 100	2 – 100
Step width (° 2θ)	0.001	0.001	0.001

Section S7.

Table S7.1. Crystallographic and refinement data (Rietveld refinement of complete crystal structures) for hydroxyapatites (space group $P6_3/m$ (176)) with different intercalated metal atoms from laboratory X-ray powder diffraction data (R_{Br} , R_p , R_{wp} and $GooF$ as defined in Topas).

Sample	SrA(0.25Cu)	SrA(0.125Cu)	SrA(0.05Cu)	SrA(0.05Cu_0.5F)
Molecular formula	$\text{Sr}_5(\text{PO}_4)_3\text{Cu}_{0.25}\text{OH}_{0.75-\delta}$	$\text{Sr}_5(\text{PO}_4)_3\text{Cu}_{0.125}\text{OH}_{0.875-\delta}$	$\text{Sr}_5(\text{PO}_4)_3\text{Cu}_{0.05}\text{OH}_{0.95-\delta}$	$\text{Sr}_5(\text{PO}_4)_3\text{Cu}_{0.05}\text{O}_{0.5}\text{H}_{0.45-\delta}\text{F}_{0.5}$
Z	2	2	2	2
$a / \text{\AA}$	9.7780(3)	9.7635(2)	9.7602(2)	9.7382(2)
$c / \text{\AA}$	7.2942(2)	7.2810(2)	7.2763(2)	7.2844(2)
R_{Br} , %	3.36	3.26	3.93	4.13
R_p , %	5.74	5.22	5.56	6.50
R_{wp} , %	8.89	8.34	8.18	9.72
$GooF$	3.50	3.31	2.70	3.11
Temperature (K)	293	293	293	293
Wavelength (\AA)	1.540596	1.540596	1.540596	1.540596
2θ – range ($^\circ$)	10 – 120	10 – 120	15 – 100	15 – 100
Step width ($^\circ 2\theta$)	0.0079	0.0079	0.0079	0.0079

Sample	CaA(0.3Cu)	CaA(0.1Cu)	SrA(0.2Ni)	SrA(0.15Zn)
Molecular formula	$\text{Ca}_5(\text{PO}_4)_3\text{Cu}_{0.3}\text{OH}_{0.7-\delta}$	$\text{Ca}_5(\text{PO}_4)_3\text{Cu}_{0.1}\text{OH}_{0.9-\delta}$	$\text{Sr}_5(\text{PO}_4)_3\text{Ni}_{0.2}\text{OH}_{0.8-\delta}$	$\text{Sr}_5(\text{PO}_4)_3\text{Zn}_{0.15}\text{OH}_{0.85-\delta}$
Z	2	2	2	2
$a / \text{\AA}$	9.4319 (3)	9.4220(2)	9.7743(2)	9.7531(2)
$c / \text{\AA}$	6.9081 (2)	6.8871(2)	7.2977(2)	7.3088(2)
R_{Br} , %	3.34	4.55	2.35	4.67
R_p , %	6.94	7.80	4.53	5.29
R_{wp} , %	10.01	10.78	6.09	7.05
$GooF$	2.18	2.37	0.95	1.68
Temperature (K)	293	293	293	293
Wavelength (\AA)	1.540596	1.540596	1.540596	1.540596
2θ – range ($^\circ$)	10 – 120	10 – 120	15 – 100	15 – 100
Step width ($^\circ 2\theta$)	0.0079	0.0079	0.01	0.01

Sample	CaA(0.1Cu_0.5F)	CaA(0.05Cu_0.5F)	CaA(0.02Cu_0.5F)	CaA(0.01Cu_0.5F)
Molecular formula	Ca ₅ (PO ₄) ₃ Cu _{0.1} O _{0.5} H _{0.4-δ} F _{0.5}	Ca ₅ (PO ₄) ₃ Cu _{0.05} O _{0.5} H _{0.45-δ} F _{0.5}	Ca ₅ (PO ₄) ₃ Cu _{0.02} O _{0.5} H _{0.48-δ} F _{0.5}	Ca ₅ (PO ₄) ₃ Cu _{0.01} O _{0.5} H _{0.49-δ} F _{0.5}
Z	2	2	2	2
a / Å	9.3977(2)	9.3954(2)	9.3941(2)	9.3932(2)
c / Å	6.8930(2)	6.8890(2)	6.8855(2)	6.8846(2)
R _{Br} , %	6.58	4.93	4.86	4.30
R _p , %	6.84	7.17	7.23	5.99
R _w p, %	9.92	10.05	10.41	8.41
GooF	2.12	2.07	2.27	2.04
Temperature (K)	293	293	293	293
Wavelength (Å)	1.540596	1.540596	1.540596	1.540596
2θ – range (°)	10 – 120	10 – 120	10 – 120	10 – 120
Step width (° 2θ)	0.0079	0.0079	0.0079	0.0079

Sample	SrA(0.1Cu-1)	SrA(0.1Cu-2)	SrA(0.1Cu-3)	SrA(0.1Cu-4)
Molecular formula	Sr ₅ (PO ₄) ₃ Cu _{0.1} OH _{0.9-δ}	Sr ₅ (PO ₄) ₃ Cu _{0.1} OH _{0.9-δ}	Sr ₅ (PO ₄) ₃ Cu _{0.1} OH _{0.9-δ}	Sr ₅ (PO ₄) ₃ Cu _{0.1} OH _{0.9-δ}
Z	2	2	2	2
a / Å	9.7689(3)	9.7647(3)	9.7599(3)	9.7559(3)
c / Å	7.2849(3)	7.2827(3)	7.2788(3)	7.2771(3)
R _{Br} , %	4.20	4.41	3.96	4.48
R _p , %	6.42	6.42	5.30	5.77
R _w p, %	9.35	9.67	8.04	9.20
GooF	4.17	3.78	3.42	4.28
Temperature (K)	293	293	293	293
Wavelength (Å)	1.540596	1.540596	1.540596	1.540596
2θ – range (°)	10 – 120	10 – 120	10 – 120	10 – 120
Step width (° 2θ)	0.0079	0.0079	0.0079	0.0079

Sample	SrA(0.3Cu-1)	SrA(0.3Cu-2)	SrA(0.3Cu-3)
Molecular formula	Sr ₅ (PO ₄) ₃ Cu _{0.3} OH _{0.7-δ}	Sr ₅ (PO ₄) ₃ Cu _{0.3} OH _{0.7-δ}	Sr ₅ (PO ₄) ₃ Cu _{0.3} OH _{0.7-δ}
Z	2	2	2
a / Å	9.7768(3)	9.7760(3)	9.7662(3)
c / Å	7.2916(3)	7.2926(3)	7.2882(3)
R _{Br} , %	6.71	6.05	5.61
R _p , %	9.99	8.60	7.52
R _w p, %	15.11	12.24	10.47
GooF	3.91	3.40	2.50
Temperature (K)	293	293	293
Wavelength (Å)	1.540596	1.540596	1.540596
2θ – range (°)	10 – 120	10 – 120	10 – 120
Step width (° 2θ)	0.0079	0.0079	0.0079

Table S7.2. Crystallographic and refinement data (Rietveld refinement of complete crystal structures) for hydroxyapatites SrA(0.1Cu-1), SrA(0.1Cu-2), SrA(0.1Cu-3), SrA(0.1Cu-4) from synchrotron X-ray powder diffraction data (R_{Br} , R_p , R_{wp} and $GooF$ as defined in Topas).

Sample	SrA(0.1Cu-1)	SrA(0.1Cu-2)	SrA(0.1Cu-3)	SrA(0.1Cu-4)
Molecular formula	$\text{Sr}_5(\text{PO}_4)_3\text{Cu}_{0.1}\text{OH}_{0.9-\delta}$	$\text{Sr}_5(\text{PO}_4)_3\text{Cu}_{0.1}\text{OH}_{0.9-\delta}$	$\text{Sr}_5(\text{PO}_4)_3\text{Cu}_{0.1}\text{OH}_{0.9-\delta}$	$\text{Sr}_5(\text{PO}_4)_3\text{Cu}_{0.1}\text{OH}_{0.9-\delta}$
Z	2	2	2	2
$a / \text{\AA}$	9.7696(3)	9.7665(3)	9.7626(3)	9.7584(3)
$c / \text{\AA}$	7.2855(3)	7.2851(3)	7.2821(3)	7.2782(3)
R_{Br} , %	4.41	4.06	4.48	3.55
R_p , %	7.55	5.70	5.78	5.28
R_{wp} , %	9.80	7.50	7.63	7.07
$GooF$	2.85	2.23	2.57	2.10
Temperature (K)	293	293	293	293
Wavelength (\AA)	0.8264	0.8264	0.8264	0.8264
2θ – range ($^\circ$)	2 – 100	2 – 100	2 – 100	2 – 100
Step width ($^\circ 2\theta$)	0.001	0.001	0.001	0.001

Section S8.

Table S8.1. Details about maximum-entropy calculations for incomplete crystal structures (without intercalated metal atoms) of investigated apatites from laboratory X-ray powder diffraction data (R_F , R_{wF} , R_G and R_{wG} as defined in BayMEM).

Sample	SrA(0.25Cu)	CaA(0.1Cu)	SrA(0.2Ni)	SrA(0.15Zn)
The grid / pixels	96×96×72			
Resolution / Å ³	0.1×0.1×0.1			
F(0 0 0)	693.48	505.40	690.39	688.38
Lagrange multiplier, λ_{FG}	50	140	100	100
MEM calculations based on F_{obs} (procrystal density for known atoms)				
χ^2_{aim}	3.0	1.8	0.4	0.3
R_F / R_{wF} , %	2.05 / 2.18	1.73 / 1.80	1.19 / 1.10	0.76 / 0.76
MEM calculations based on F_{obs} (flat prior)				
χ^2_{aim}	6.0	2.7	0.7	0.4
R_F / R_{wF} , %	2.81 / 3.08	1.99 / 2.20	1.42 / 1.46	0.89 / 0.87
MEM calculations based on $F_{obs} + G$ and $F_{LeBail} + G$				
$\chi^2_{aim} (F_{obs}+G)$	1.4	0.4	0.1	0.2
R_F / R_{wF} , % ($F_{obs}+G$)	2.52 / 2.56	1.73 / 1.62	1.22 / 1.03	1.30 / 1.00
R_G / R_{wG} , % ($F_{obs}+G$)	1.10 / 1.31	0.53 / 0.66	0.59 / 0.50	0.66 / 0.70
$\chi^2_{aim} (F_{LeBail}+G)$	1.0	0.4	0.1	0.1
R_F / R_{wF} , % ($F_{LeBail}+G$)	1.99 / 2.40	1.65 / 1.51	1.87 / 1.38	0.87 / 0.62
R_G / R_{wG} , % ($F_{LeBail}+G$)	0.93 / 0.99	0.57 / 0.74	0.09 / 0.10	0.75 / 0.85
No. of unique reflection	54	47	37	18
No. of overlapping reflection	222	198	190	192
No. of groups of the overlapping reflections	86	75	64	60

Sample	CaA(0.1Cu_0.5F)	CaA(0.05Cu_0.5F)	CaA(0.02Cu_0.5F)	CaA(0.01Cu_0.5F)
The grid / pixels	96×96×72			
Resolution / Å ³	0.1×0.1×0.1			
F(0 0 0)	505.40	502.69	501.07	500.54
Lagrange multiplier, λ_{FG}	50	50	50	50
MEM calculations based on F_{obs} (procrystal density for known atoms)				
χ^2_{aim}	0.5	0.6	0.1	0.1
R_F / R_{wF} , %	0.96 / 1.05	0.99 / 1.13	0.37 / 0.45	0.36 / 0.40
MEM calculations based on F_{obs} (flat prior)				
χ^2_{aim}	2.0	0.9	1.0	1.0
R_F / R_{wF} , %	1.83 / 2.11	1.17 / 1.39	1.17 / 1.43	1.05 / 1.20
MEM calculations based on $F_{obs} + G$ and $F_{LeBail} + G$				
$\chi^2_{aim} (F_{obs}+G)$	0.5	0.2	0.1	0.1
R_F / R_{wF} , % ($F_{obs}+G$)	1.60 / 1.72	0.96 / 1.01	0.73 / 0.78	0.70 / 0.71
R_G / R_{wG} , % ($F_{obs}+G$)	0.70 / 0.84	0.44 / 0.60	0.30 / 0.37	0.35 / 0.44
$\chi^2_{aim} (F_{LeBail}+G)$	0.5	0.3	0.1	0.1
R_F / R_{wF} , % ($F_{LeBail}+G$)	1.55 / 1.57	1.38 / 1.29	0.79 / 0.79	0.83 / 0.76
R_G / R_{wG} , % ($F_{LeBail}+G$)	0.77 / 0.97	0.60 / 0.71	0.30 / 0.38	0.34 / 0.41
No. of unique reflection	58	56	54	55
No. of overlapping reflection	187	189	191	190
No. of groups of the overlapping reflections	82	79	79	79

Sample	SrA(0.1Cu-1)	SrA(0.1Cu-3)	SrA(0.1Cu-4)
The grid / pixels	96×96×72		
Resolution / Å ³	0.1×0.1×0.1		
F(0 0 0)	685.38	685.38	685.38
Lagrange multiplier, λ_{FG}	50	50	50
MEM calculations based on F_{obs} (procrystal density for known atoms)			
χ^2_{aim}	1.0	0.9	0.4
R_F / R_{wF} , %	1.14 / 1.22	1.09 / 1.17	0.64 / 0.73
MEM calculations based on F_{obs} (flat prior)			
χ^2_{aim}	1.5	1.3	1.6
R_F / R_{wF} , %	1.32 / 1.50	1.23 / 1.40	1.24 / 1.45
MEM calculations based on $F_{obs} + G$ and $F_{LeBail} + G$			
$\chi^2_{aim} (F_{obs}+G)$	0.2	0.2	0.2
R_F / R_{wF} , % ($F_{obs}+G$)	0.87 / 0.93	0.96 / 0.97	0.70 / 0.79
R_G / R_{wG} , % ($F_{obs}+G$)	0.40 / 0.44	0.39 / 0.44	0.44 / 0.50
$\chi^2_{aim} (F_{LeBail}+G)$	0.3	0.3	6.0
R_F / R_{wF} , % ($F_{LeBail}+G$)	1.00 / 1.17	1.19 / 1.17	3.15 / 3.72
R_G / R_{wG} , % ($F_{LeBail}+G$)	0.49 / 0.55	0.51 / 0.55	2.83 / 3.17
No. of unique reflection	60	56	51
No. of overlapping reflection	216	220	225
No. of groups of the overlapping reflections	90	91	84

Table S8.2. Details about maximum-entropy calculations for incomplete crystal structures (without intercalated metal atoms) of investigated apatites from synchrotron X-ray powder diffraction data with resolution $\sin\theta/\lambda = 0.93$ (R_F , R_{wF} , R_G and R_{wG} as defined in BayMEM).

Sample	SrA(0.1Cu-1)	SrA(0.1Cu-3)	SrA(0.1Cu-4)
The grid / pixels	96×96×72		
Resolution / \AA^3	0.1×0.1×0.1		
F(0 0 0)	685.38	685.38	685.38
Lagrange multiplier, λ_{FG}	50	50	50
MEM calculations based on F_{obs} (procrystal density for known atoms)			
χ^2_{aim}	1.0	0.9	0.2
R_F / R_{wF} , %	1.34 / 0.16	1.33 / 1.55	0.63 / 0.69
MEM calculations based on F_{obs} (flat prior)			
χ^2_{aim}	3.5	2.8	2
R_F / R_{wF} , %	2.22 / 2.99	2.05 / 2.74	1.63 / 2.20
MEM calculations based on $F_{\text{obs}} + G$ and $F_{\text{LeBail}} + G$			
χ^2_{aim} ($F_{\text{obs}}+G$)	0.2	0.2	0.1
R_F / R_{wF} , % ($F_{\text{obs}}+G$)	1.40 / 1.49	1.30 / 1.45	1.17 / 1.13
R_G / R_{wG} , % ($F_{\text{obs}}+G$)	0.63 / 0.73	0.66 / 0.75	0.44 / 0.51
χ^2_{aim} ($F_{\text{LeBail}}+G$)	1.3	0.7	1.5
R_F / R_{wF} , % ($F_{\text{LeBail}}+G$)	2.77 / 3.31	2.03 / 2.46	2.63 / 2.57
R_G / R_{wG} , % ($F_{\text{LeBail}}+G$)	1.67 / 1.99	1.20 / 1.48	2.35 / 2.49
No. of unique reflection	89	99	71
No. of overlapping reflection	1324	1314	1341
No. of groups of the overlapping reflections	351	375	306

Table S8.3. Details about maximum-entropy calculations for incomplete crystal structures (without intercalated metal atoms) of investigated apatites from synchrotron X-ray powder diffraction data with resolution $\sin\theta/\lambda = 0.65$ (R_F , R_{wF} , R_G and R_{wG} as defined in BayMEM).

Sample	SrA(0.1Cu-1)	SrA(0.1Cu-3)	SrA(0.1Cu-4)
The grid / pixels	96×96×72		
Resolution / \AA^3	0.1×0.1×0.1		
F(0 0 0)	685.38	685.38	685.38
Lagrange multiplier, λ_{FG}	50	50	50
MEM calculations based on F_{obs} (procrystal density for known atoms)			
χ^2_{aim}	0.6	0.1	0.2
R_F / R_{wF} , %	0.93 / 1.02	0.40 / 0.43	0.55 / 0.58
MEM calculations based on F_{obs} (flat prior)			
χ^2_{aim}	2.0	1.5	1.6
R_F / R_{wF} , %	1.57 / 1.87	1.39 / 1.67	1.37 / 1.64
MEM calculations based on $F_{\text{obs}} + G$ and $F_{\text{LeBail}} + G$			
χ^2_{aim} ($F_{\text{obs}}+G$)	0.1	0.2	0.1
R_F / R_{wF} , % ($F_{\text{obs}}+G$)	0.77 / 0.69	1.05 / 0.99	0.81 / 0.74
R_G / R_{wG} , % ($F_{\text{obs}}+G$)	0.34 / 0.40	0.49 / 0.58	0.35 / 0.39
χ^2_{aim} ($F_{\text{LeBail}}+G$)	0.4	0.2	0.4
R_F / R_{wF} , % ($F_{\text{LeBail}}+G$)	1.41 / 1.40	0.89 / 1.00	0.75 / 0.75
R_G / R_{wG} , % ($F_{\text{LeBail}}+G$)	0.63 / 0.79	0.49 / 0.56	0.77 / 1.02
No. of unique reflection	79	79	62
No. of overlapping reflection	416	416	433
No. of groups of the overlapping reflections	160	159	142

Table S8.4. Details about maximum-entropy calculations for incomplete crystal structures (without intercalated metal atoms) of investigated apatites from synchrotron X-ray powder diffraction data with resolution $\sin\theta/\lambda = 0.55$ (R_F , R_{wF} , R_G and R_{wG} as defined in BayMEM).

Sample	SrA(0.1Cu-1)	SrA(0.1Cu-3)	SrA(0.1Cu-4)
The grid / pixels	96×96×72		
Resolution / \AA^3	0.1×0.1×0.1		
F(0 0 0)	685.38	685.38	685.38
Lagrange multiplier, λ_{FG}	50	50	50
MEM calculations based on F_{obs} (procrystal density for known atoms)			
χ^2_{aim}	0.1	0.1	0.1
R_F / R_{wF} , %	0.39 / 0.40	0.40 / 0.42	0.38 / 0.40
MEM calculations based on F_{obs} (flat prior)			
χ^2_{aim}	1.0	0.8	1.0
R_F / R_{wF} , %	1.10 / 1.28	0.99 / 1.17	1.06 / 1.25
MEM calculations based on $F_{\text{obs}} + G$ and $F_{\text{LeBail}} + G$			
χ^2_{aim} ($F_{\text{obs}}+G$)	0.1	0.1	0.1
R_F / R_{wF} , % ($F_{\text{obs}}+G$)	0.73 / 0.63	0.72 / 0.63	0.72 / 0.63
R_G / R_{wG} , % ($F_{\text{obs}}+G$)	0.31 / 0.36	0.33 / 0.37	0.33 / 0.38
χ^2_{aim} ($F_{\text{LeBail}}+G$)	0.2	0.2	3.3
R_F / R_{wF} , % ($F_{\text{LeBail}}+G$)	0.86 / 0.94	0.76 / 0.85	1.62 / 2.39
R_G / R_{wG} , % ($F_{\text{LeBail}}+G$)	0.44 / 0.48	0.48 / 0.54	1.99 / 2.69
No. of unique reflection	66	65	54
No. of overlapping reflection	253	252	266
No. of groups of the overlapping reflections	107	108	102

Section S9.

Table S9.1. Details about maximum-entropy calculations (based on $F_{\text{obs}}+G$) for complete crystal structures of investigated apatites from laboratory X-ray powder diffraction data (R_F , R_{wF} , R_G and R_{wG} as defined in BayMEM).

Sample	SrA(0.25Cu)	SrA(0.125Cu)	SrA(0.05Cu)	SrA(0.05Cu_0.5F)
The grid / pixels	96×96×72			
Resolution / Å ³	0.1×0.1×0.1			
F(0 0 0)	693.48	685.28	682.68	690.68
Lagrange multiplier, λ_{FG}	50	40	40	40
χ^2_{aim}	0.4	0.4	0.4	0.2
R_F / R_{wF} , %	1.13/1.14	0.97/1.02	0.77/0.96	0.54/0.65
R_G / R_{wG} , %	0.69/0.81	0.73/0.87	0.79/0.88	0.54/0.62
No. of unique reflection	54	54	44	46
No. of overlapping reflection	222	220	238	230
No. of groups of the overlapping reflections	86	85	91	80

Sample	CaA(0.3Cu)	CaA(0.1Cu)	SrA(0.2Ni)	SrA(0.15Zn)
The grid / pixels	96×96×72			
Resolution / Å ³	0.1×0.1×0.1			
F(0 0 0)	516.19	505.40	690.39	688.38
Lagrange multiplier, λ_{FG}	130	140	100	100
χ^2_{aim}	0.3	0.3	0.2	0.2
R_F / R_{wF} , %	1.37/1.22	1.42/1.29	1.42/1.30	1.54/1.16
R_G / R_{wG} , %	0.65/0.74	0.54/0.68	0.93/0.77	0.61/0.68
No. of unique reflection	51	47	37	18
No. of overlapping reflection	195	198	190	192
No. of groups of the overlapping reflections	80	75	64	60

Sample	CaA(0.1Cu_0.5F)	CaA(0.05Cu_0.5F)	CaA(0.02Cu_0.5F)	CaA(0.01Cu_0.5F)
The grid / pixels	96×96×72			
Resolution / Å ³	0.1×0.1×0.1			
F(0 0 0)	505.40	502.69	501.07	500.54
Lagrange multiplier, λ_{FG}	50	50	50	50
χ^2_{aim}	0.2	0.2	0.2	0.2
R _F / R _{wF} , %	0.88/0.95	1.11/1.06	0.57/0.68	0.48/0.67
R _G / R _{wG} , %	0.51/0.60	0.48/0.52	0.45/0.52	0.41/0.45
No. of unique reflection	58	56	54	55
No. of overlapping reflection	187	189	191	190
No. of groups of the overlapping reflections	82	79	79	79

Sample	SrA(0.1Cu-1)	SrA(0.1Cu-2)	SrA(0.1Cu-3)	SrA(0.1Cu-4)
The grid / pixels	96×96×72			
Resolution / Å ³	0.1×0.1×0.1			
F(0 0 0)	685.38	685.38	685.38	685.38
Lagrange multiplier, λ_{FG}	50	50	50	50
χ^2_{aim}	0.4	0.4	0.4	0.4
R _F / R _{wF} , %	0.90/1.01	1.22/1.29	0.96/1.09	0.93/1.03
R _G / R _{wG} , %	0.66/0.79	0.62/0.70	0.67/0.77	0.69/0.76
No. of unique reflection	60	55	56	51
No. of overlapping reflection	216	221	220	225
No. of groups of the overlapping reflections	90	91	91	84

Sample	SrA(0.3Cu-1)	SrA(0.3Cu-2)	SrA(0.3Cu-3)
The grid / pixels	96×96×72		
Resolution / Å ³	0.1×0.1×0.1		
F(0 0 0)	696.18	696.18	696.18
Lagrange multiplier, λ_{FG}	50	50	50
χ^2_{aim}	0.4	0.4	0.4
R _F / R _{wF} , %	0.95/1.05	1.01/1.08	1.06/1.16
R _G / R _{wG} , %	0.82/0.99	0.78/0.92	0.88/0.90
No. of unique reflection	42	44	40
No. of overlapping reflection	234	232	236
No. of groups of the overlapping reflections	86	90	81

Table S9.2. Details about maximum-entropy calculations (based on $F_{\text{obs}}+G$) for complete crystal structures of investigated apatites from synchrotron X-ray powder diffraction data with resolution $\sin\theta/\lambda = 0.93$ (R_F , R_{wF} , R_G and R_{wG} as defined in BayMEM).

Sample	SrA(0.1Cu-1)	SrA(0.1Cu-2)	SrA(0.1Cu-3)	SrA(0.1Cu-4)
The grid / pixels	96×96×72			
Resolution / Å ³	0.1×0.1×0.1			
F(0 0 0)	685.38	685.38	685.38	685.38
Lagrange multiplier, λ_{FG}	50	50	50	50
χ^2_{aim}	0.4	0.4	0.4	0.4
R_F / R_{wF} , %	1.38/1.86	1.37/1.84	1.26/1.67	1.38/1.76
R_G / R_{wG} , %	0.96/1.10	0.97/1.16	0.99/1.17	0.99/1.14
No. of unique reflection	89	104	99	71
No. of overlapping reflection	1324	1309	1314	1341
No. of groups of the overlapping reflections	351	381	375	306

Table S9.3. Details about maximum-entropy calculations (based on $F_{\text{obs}}+G$) for complete crystal structures of investigated apatites from synchrotron X-ray powder diffraction data with resolution $\sin\theta/\lambda = 0.65$ (R_F , R_{wF} , R_G and R_{wG} as defined in BayMEM).

Sample	SrA(0.1Cu-1)	SrA(0.1Cu-2)	SrA(0.1Cu-3)	SrA(0.1Cu-4)
The grid / pixels	96×96×72			
Resolution / Å ³	0.1×0.1×0.1			
F(0 0 0)	685.38	685.38	685.38	685.38
Lagrange multiplier, λ_{FG}	50	50	50	50
χ^2_{aim}	0.4	0.4	0.4	0.4
R_F / R_{wF} , %	0.97/1.20	1.05/1.24	1.00/1.16	1.07/1.17
R_G / R_{wG} , %	0.74/0.87	0.79/0.91	0.79/0.92	0.80/0.90
No. of unique reflection	79	81	79	62
No. of overlapping reflection	416	414	416	433
No. of groups of the overlapping reflections	160	163	159	142

Table S9.4. Details about maximum-entropy calculations (based on $F_{\text{obs}}+G$) for complete crystal structures of investigated apatites from synchrotron X-ray powder diffraction data with resolution $\sin\theta/\lambda = 0.55$ (R_F , R_{wF} , R_G and R_{wG} as defined in BayMEM).

Sample	SrA(0.1Cu-1)	SrA(0.1Cu-2)	SrA(0.1Cu-3)	SrA(0.1Cu-4)
The grid / pixels	96×96×72			
Resolution / Å ³	0.1×0.1×0.1			
F(0 0 0)	685.38	685.38	685.38	685.38
Lagrange multiplier, λ_{FG}	50	50	50	50
χ^2_{aim}	0.4	0.4	0.4	0.4
R_F / R_{wF} , %	0.81 / 1.04	0.86 / 1.03	0.91 / 1.03	0.95 / 1.00
R_G / R_{wG} , %	0.72 / 0.83	0.79 / 0.90	0.74 / 0.87	0.75 / 0.87
No. of unique reflection	66	65	65	54
No. of overlapping reflection	253	252	252	266
No. of groups of the overlapping reflections	107	108	108	102

Section S10. References

Cheary, R. W.; Coelho, A. A. A fundamental parameters approach to X-ray line-profile fitting // *J. Appl. Cryst.* **1992**, 25, 109 – 121.

Hofmann, A.; Netzel, J.; van Smaalen, S. Accurate charge density of trialanine: a comparison of the multipole formalism and the maximum entropy method (MEM) // *Acta Cryst.* **2007**, B63, 285 – 295.

Karpov, A. S.; Nuss, J.; Jansen, M.; Kazin, P. E.; Tretyakov, Yu. D. Synthesis, crystal structure and properties of calcium and barium hydroxyapatites containing copper ions in hexagonal channels // *Solid State Science.* **2003**, 5, 1277 – 1283.

Kazin, P. E.; Karpov, A. S.; Jansen, M.; Nuss, J.; Tretyakov, Yu. D. Crystal structure and properties of strontium phosphate apatite with oxocuprate ions in hexagonal channels // *Z. Anorg. Allg. Chem.* **2003**, 629, 344 – 352.

Kazin, P. E.; Gazizova, O. R.; Karpov, A. S.; Jansen, M.; Tretyakov, Yu. D. Incorporation of 3d-metal ions in the hexagonal channels of the $\text{Sr}_5(\text{PO}_4)_3\text{OH}$ apatite // *Solid State Science.* **2007**, 9, 82 – 87.

Kazin, P. E.; Zykin, M. A.; Tretyakov, Yu. D.; Jansen, M. Synthesis and properties of colored copper-containing apatites of composition $\text{Ca}_5(\text{PO}_4)_3\text{Cu}_y\text{O}_y + \delta(\text{OH})_{0.5 - y - \delta}\text{X}_{0.5}$ ($\text{X} = \text{OH}, \text{F}, \text{Cl}$) // *Russ. J. Inorg. Chem.* **2008**, 53, 409 – 414.

Kazin, P. E.; Zykin, M. A.; et al. Will be published

Parker, J. E.; Thompson, S. P.; Cobb, T. M.; Yuan, F.; Potter, J.; Lennie, A. R.; Alexander, S.; Tighe, C. J.; Darr, J. A.; Cockcroft, J. C.; Tang, C. C. High-throughput powder diffraction on beamline I11 at Diamond // *J. Appl. Cryst.* **2011**, 44, 102 – 110.

Sakata, M.; Sato, M. Accurate structure analysis by the maximum-entropy method // *Acta Cryst.* **1990**, A46, 263 – 270.

van Smaalen, S.; Palatinus, L.; Schneider, M. The maximum entropy method in superspace // *Acta Cryst.* **2003**, A59, 459 – 469.

Thompson, S. P.; Parker, J. E.; Marchal, J.; Potter, J.; Birt, A.; Yuan, F.; Fearn, R. D.; Lennie, A. R.; Street, S. R.; Tang, C. C. Fast X-ray powder diffraction on I11 at Diamond // *J. Synchrotron Rad.* **2011**, 18, 637 – 648.

Thompson, S. P.; Parker, J. E.; Potter, J.; Hill, T. P.; Birt, A.; Cobb, T. M.; Yuan, F.; Tang, C. C. Beamline I11 at Diamond: A new instrument for high resolution powder Diffraction // *Rev. Sci. Instrum.* **2009**, 80, 075107-1 – 075107-9.

TOPAS version 4.1 (**2007**), Bruker-AXS, Karlsruhe, Germany.